

# Gamma-Ray Summary Report

J. Buckley\*

*Washington University, St. Louis*

T. Burnett†

*University of Washington*

G. Sinnis‡

*Los Alamos National Laboratory*

P. Coppi§

*Yale University*

P. Gondolo¶

*Case Western Reserve University*

J. Kapusta\*\*

*University of Minnesota*

J. McEnery††

*University of Wisconsin*

J. Norris‡‡

*NASA/Goddard Space Flight Center*

P. Ullio§§

*SISSA*

D.A. Williams

*University of California Santa Cruz¶¶*

(Dated: November 6, 2018)

This paper reviews the field of gamma-ray astronomy and describes future experiments and prospects for advances in fundamental physics and high-energy astrophysics through gamma-ray measurements. We concentrate on recent progress in the understanding of active galaxies, and the use of these sources as probes of intergalactic space. We also describe prospects for future experiments in a number of areas of fundamental physics, including: searches for an annihilation line from neutralino dark matter, understanding the energetics of supermassive black holes, using AGNs as cosmological probes of the primordial radiation fields, constraints on quantum gravity, detection of a new spectral component from GRBs, and the prospects for detecting primordial black holes.

## I. INTRODUCTION

With new experiments such as GLAST and VERITAS on the horizon, we are entering an exciting period for gamma-ray astronomy. The gamma-ray waveband has provided a new spectral window on the universe

---

\*Electronic address: buckley@wuphys.wustl.edu

†Electronic address: tburnett@u.washington.edu

‡Electronic address: Gus@lanl.gov

§Electronic address: coppi@astro.yale.edu

¶Electronic address: pxg26@po.cwru.edu

\*\*Electronic address: kapusta@physics.umn.edu

††Electronic address: mcenery@titus.physics.wisc.edu

‡‡Electronic address: jnorris@lheapop.gsfc.nasa.gov

§§Electronic address: ullio@he.sissa.it

¶¶Electronic address: daw@scipp.ucsc.edu

and has already resulted in dramatic progress in our understanding of high energy astrophysical phenomena. At these energies the universe looks quite different than when viewed with more traditional astronomical techniques. The sources of high energy gamma rays are limited to the most extreme places in the universe: the remnants of exploding stars, the nonthermal Nebulae surrounding pulsars, the ultra-relativistic jets emerging from supermassive black holes at the center of active galaxies, and the still mysterious gamma-ray bursters.

While understanding these objects is of intrinsic interest (how does nature accelerate particles to such high energies? how do particles and fields behave in the presence of strong gravitational fields?), these objects can also be used as probes of the radiation fields in the universe and possibly of spacetime itself. In this case, the astrophysics of the object is a confounding factor that must be understood to produce a quantitative measurement or a robust upper limit. While some may view this as a limitation of such *indirect* astrophysical measurements, in most cases there are no earth-bound experiments that can probe the fundamental laws of physics at the energy scales available to gamma-ray instruments.

Gamma-ray astronomy has developed along two separate paths. From the ground, simple, inexpensive experiments were built in the 1950's to observe the Cherenkov light generated by extensive air showers generated by photons with energies above several TeV. Despite decades of effort it was not until the late 1980's that a source of TeV photons was observed. There are now roughly 10 known sources of TeV gamma rays, three galactic sources and at least three active galaxies. From space, the COS-B satellite, launched in 1975, observed the first sources of cosmic gamma rays at energies above 70 MeV. The launch of the Compton Gamma Ray Observatory (CGRO) in 1991, with the *Energetic Gamma Ray Experiment Telescope* (EGRET) instrument, brought the field to maturity. Whereas COS-B discovered a handful of sources, EGRET observed over 65 active galaxies[1], seven pulsars, many gamma-ray bursts, and over 60 sources that have no known counterparts at other wavelengths.

The disparity in the development of the two techniques can be traced to the extremely low fluxes of particles present above a TeV ( $\sim 4\gamma$  football field $^{-1}$  hr $^{-1}$ ) and the cosmic-ray background. Above the earth's atmosphere, one can surround a gamma-ray detector with a veto counter that registers the passage of charged particles. From the ground, one is forced to infer the nature of the primary particle by observing the secondary radiation generated as the extensive air shower develops. It was not until such a technique was developed for air Cherenkov telescopes [2], that sources of TeV photons were discovered. Despite these difficulties a new generation of ground-based instruments is under development that will have a sensitivity that will rival that of space-based instruments. At the same time a space-based instrument, GLAST, with a relatively large area ( $\sim 1\text{m}^2$ ) and excellent energy and angular resolution is scheduled to be launched in 2005.

In this paper we will give a brief survey of the gamma-ray universe and demonstrate some of the fundamental measurements (relevant to particle physicists) that can be made using distant objects that emit high-energy photons. What will hopefully become clear from this exposition are some development paths for future instruments. The need to see to the far reaches of the universe, makes a compelling case for ground-based instruments with energy thresholds as low as 10 GeV. The need to detect and study the many transient phenomena in the universe makes a compelling case for the development of an instrument that can continually monitor the entire overhead sky at energies above  $\sim 100$  GeV with sensitivities approaching that of the next generation of pointed instruments.

As with any new branch of astronomy, it is impossible to predict what knowledge will ultimately be gained from studying the universe in a different waveband, but early results hint at a rich future. New and planned instruments with greatly increased sensitivity will allow us to look farther into the universe and deeper into the astrophysical objects that emit gamma rays. Gamma-ray astronomy can be used to study the most extreme environments that exist in the universe, and may also provide a number of unique laboratories for exploring the fundamental laws of physics at energies beyond the reach of earth-bound particle accelerators.

## II. PHYSICS GOALS OF GAMMA RAY ASTRONOMY

### A. Active Galactic Nuclei

Active galactic nuclei (AGN) are believed to be supermassive black holes,  $10^8 - 10^{10} M_{\odot}$ , accreting matter from the nucleus of a host galaxy. The accretion of matter onto a black hole is a very efficient process, capable of releasing  $\sim 10\%$  of the rest energy the infalling matter ( $\sim 40\%$  for a maximally rotating black hole). (For comparison fusion burning in stars releases  $\sim 0.7\%$  of the rest energy.) Radio loud AGN emit jets of relativistic particles, presumably along the rotation axis of the spinning black hole. The COS-B instrument observed the first AGN in the gamma-ray regime ( $E > 100$  MeV), 3C273. But it was not until the launch of the CGRO and EGRET that many AGN could be studied in the gamma-ray regime. More recently, ground-based instruments have extended these observations into the TeV energy band. The energy output of these objects in gamma rays is of order  $10^{45}$  ergs s $^{-1}$ , and many of these objects emit most of their energy into gamma rays. The relativistic

motion has several effects: 1) the energy of the photons is blue-shifted for an observer at rest (us), 2) the timescale is Lorentz contracted (further increasing the apparent luminosity), and 3) the relativistic beaming suppresses photon interactions. Thus, one expects that AGN observed in the TeV regime should have their jets nearly aligned with our line-of-sight.

The types of AGN detected at high energies, which include flat spectrum radio quasars (FSRQs) and BL Lacertae (BL Lac) objects, are collectively referred to as *blazars*. The Whipple Observatory 10m atmospheric Cherenkov telescope demonstrated that the emission spectra of several blazars extend into TeV energies. Two of these detections (Markarian 421 and Markarian 501) have been confirmed by independent experiments (CAT and HEGRA), at significance levels of between  $20\sigma$  in a half hour to  $80\sigma$  for a season.

Blazar emission is dominated by highly variable, non-thermal continuum emission from an unresolved nucleus. The broadband emission and high degree of polarization suggest synchrotron radiation extending from radio up to UV or even hard X-ray energies. The short variability timescales and high luminosities are thought to result from highly relativistic outflows along jets pointed very nearly along our line of sight. The spectral energy distributions (SEDs) of these objects have a double-peaked shape (see Figure 1) with a synchrotron component that peaks in the UV or X-ray band, and a second component typically rising in the X-ray range and peaking at energies between  $\sim 1$  MeV and 1 TeV [3]. The most natural explanation of the second peak is inverse-Compton scattering of ambient or synchrotron photons [4] although other possibilities such as proton-induced cascades have not been ruled out [5]. These two models have somewhat complementary strengths and weaknesses. Since electrons are lighter than protons, they can be confined in a smaller acceleration region but lose energy more quickly (by synchrotron and IC emission), making it difficult to accelerate electrons to extreme energies. For hadronic models, very high energies can be attained given sufficient time, a large acceleration region and high magnetic fields. However, the short variability timescales, implying short acceleration times and compact regions are difficult to explain. In addition, the electron models make natural predictions on the correlation between X-ray and gamma ray luminosities. While it has been claimed that proton models can be constructed that explain these correlations, detailed calculations have not appeared in the literature.

Whipple observations of the vast majority of EGRET blazars have yielded only upper limits [6, 7, 8]; Mrk 421 ( $z = 0.031$ ) [9] being the exception. Subsequent searches for emission from X-ray bright BL Lac objects has led to the detection of Mrk 501 ( $z = 0.034$ ) [10], and four other as yet unconfirmed sources [1ES 2344+514 ( $z = 0.044$ ) [11], 1ES 2155-304 ( $z = 0.117$ ) [12], 1ES1959+650 ( $z = 0.048$ ) [13] and 1H1426+428 ( $z = 0.13$ ) [14]]. The SEDs observed for these sources show higher energy synchrotron and  $\gamma$ -ray peaks, and comparable power output at the synchrotron and  $\gamma$ -ray peak.

These observations are well described by the classification scheme of Padovani and Giommi [15]. The AGN detected by EGRET are all radio-loud, flat-spectrum radio sources and lie at redshifts between 0.03 and 2.28. They are characterized by two component spectra with peak power in the infrared to optical waveband and in the 10 MeV to GeV range. For many of the GeV blazars, the total power output of these sources peaks in the gamma-ray waveband.

The objects detected at VHE, appear to form a new class distinct from the EGRET sources. All are classified as *high-energy peaked [15] BL Lacs (HBLs)* defined as sources with their synchrotron emission peaked in the UV/X-ray band and gamma-ray emission peaking in the  $\sim 100$  GeV regime (see, e.g., Fig. 1). The correspondence of the position of the peak of the synchrotron and  $\gamma$ -ray energy is naturally explained in models where the same population of electrons produces both spectral components. Proton induced cascade models [5] might also reproduce the spectra, but have no natural correlation in the cutoff energy of the two components, or the observed correlated variability.

Another difference in the VHE detections is that only the nearest sources with redshifts  $z \lesssim 0.1$  have been detected. The sensitivity of EGRET for a one-year exposure is comparable to that of Whipple for a 50 hour exposure for a source with spectral index of 2.2. The failure of ACTs to detect any but the nearest AGNs therefore requires a cut-off in the  $\gamma$ -ray spectra of the EGRET sources between 10 GeV and a few hundred GeV. This cutoff could be intrinsic to the electron acceleration mechanism, due to absorption of ambient photons from the accreting nuclear region [16], or caused by absorption via pair production with the diffuse extragalactic background radiation [17, 18]. While the latter mechanism establishes an energy-dependent gamma-ray horizon it can also be used to measure the radiation fields that fill intergalactic space.

In the framework of Fossati et al., [19] the low energy peaked EGRET BL Lacs (LBLs) correspond to AGNs with a more luminous nuclear emission component than HBLs. The relatively high ambient photon density in the LBLs is up-scattered by relativistic electrons to  $\gamma$ -ray energies. With high enough ambient photon densities, the resulting inverse-Compton emission can exceed that resulting from the up-scattering of synchrotron photons. This accounts for the observation of relatively high levels of gamma-ray emission, dominating the power output over the entire spectrum.

The higher luminosity could also shut down the acceleration process at lower energies. For lack of another viable hypothesis, consider the common hypothesis that the energetic particles in AGNs come from electrons

or protons accelerated by relativistic shocks traveling down the AGN jets. In the model of diffusive shock acceleration (essentially the first order Fermi process), particles are accelerated as they are scattered from magnetic irregularities on either side of a shock. For strong, non-relativistic shocks, a constant escape probability with each shock crossing results in an  $\sim E^{-2}$  spectrum, close to that observed. More realistic models including nonlinear effects lead to slightly steeper spectra; if the shock velocity is relativistic the spectral index may range from 1.7 to 2.4. In any event, an electron spectrum  $\sim E^{-\gamma}$  will give rise to synchrotron radiation with a spectral index  $\alpha = (\gamma - 1)/2$ , in good agreement with observations.

The maximum energy attainable is given by equating the rate of energy loss from synchrotron emission or inverse-Compton emission to the acceleration rate as given by the shock parameters. In the low-energy peaked objects, it is thought that high ambient photon densities result in inverse-Compton losses that dominate over synchrotron losses and limit the maximum electron energy achieved by shock acceleration. Thus one also obtains a natural explanation for the lower energies of the peak synchrotron and IC power in these objects. In HBLs, the ambient photon fields are presumably weaker and self-Compton emission dominates over Comptonization of external photons (EC). Electrons can reach higher energies by shock acceleration, and the peaks in the SED move to higher energies and have more nearly equal peak power. This model is consistent with the data and serves as a useful paradigm for searching for new VHE sources.

The SEDs shown in Fig. 1, combine the results of a number of different measurements of the X-ray and VHE spectra of Mrk 501, and compare them with simple synchrotron self-Compton (SSC) models (see Buckley [20] and references therein). The agreement between the spectral measurements and the model is exceptionally good for Mrk 501.

### 1. Multiwavelength Observations: Variability

Data taken on Mrk 421 over the years 1995 [21] to 2001 [22] show that the  $\gamma$ -ray emission is characterized by a succession of approximately hour-long flares with relatively symmetric profiles (see Figure 2).

While most of the multiwavelength observations of Mrk 421 show evidence for correlated X-ray and gamma ray variability, the nature of the correlation is unclear and the data have traditionally undersampled the variability. However, a multi-wavelength campaign conducted on Mrk 501 in 1997 revealed a strong correlation between TeV  $\gamma$ -rays and soft X-rays (the 50–500 keV band detected by OSSE) (Fig. 1).

Recent multiwavelength observations of Mrk 421 made during the period March 18, 2001 to April 1, 2001 with the Whipple gamma-ray telescope, and the Proportional Counter Array (PCA) detector on the Rossi X-ray Timing Explorer (RXTE) better sample the rapid variability of Mrk 421. Key to the success of this campaign is the nearly continuous  $> 330$  ks exposure with RXTE [23]. Numerous ground-based atmospheric Cherenkov and optical observations were scheduled during this period to improve the temporal coverage in the optical and VHE bands. Frequent correlated hour-scale X-ray and  $\gamma$ -ray flares were observed. Fig. 2 shows a subset of these data showing the close correlation of the well-sampled TeV and X-ray (2–10 keV) lightcurves on March 19, 2001 [22].

Leptonic models provide a natural explanation of the correlated X-ray and gamma-ray flares, and can reproduce the shape of the flare spectrum. The simplest model for blazar emission is the one-zone synchrotron self-Compton (SSC) model where energetic electrons in a compact emission region up-scatter their own synchrotron radiation. As shown in Fig. 1, such a model results in surprisingly good fits to the Mrk 501 SED. In the SSC model, the intensity of the synchrotron radiation is proportional to the magnetic energy density and the number density of electrons  $I_{\text{synch}} \propto n_e$ . Since these same electrons up-scatter this radiation, the IC emission scales as  $I_{\text{IC}} \propto n_e^2$ . Thus we expect  $I_{\text{IC}} \propto I_{\text{synch}}^2$ .

Krawczynski et al., [24] examined the correlation of TeV  $\gamma$ -ray and X-ray intensity for several strong flares of Mrk 501 in 1997. The results, plotted in Figure 3, show evidence for such a quadratic dependence. (However the possibility of a baseline level of the X-ray emission can not be excluded.) While the interpretation of these observations is not unambiguous, this analysis is an important example of what can be learned with continued multiwavelength studies of AGNs.

How do these observations constrain the alternative hypothesis that proton induced cascades (PIC), not electrons, are responsible for the gamma-ray emission? In the hadronic models of Mannheim and collaborators, the gamma-ray emission typically comes from synchrotron emission from extremely energetic, secondary electrons produced in hadronic cascades. Since a viable hadronic target for  $pp \rightarrow pp\pi$  appears to be lacking (except perhaps in the broad line clouds), the assumption is made that the cascade begins with ultrarelativistic particles interacting with ambient photons to produce pions. This implies proton energies in excess of  $10^{16}$  eV. The neutral pions presumably give rise to gamma rays and electromagnetic cascades, while the charged pions could give a neutrino signal. These models have attracted much interest since, in the most optimistic cases, these models may produce an observable neutrino signal and may provide a mechanism for producing the ultra-high energy cosmic rays. If the sources are *optically thick* to the emerging protons (i.e., they absorb some fraction

This figure is available as p42\_fig1a.gif

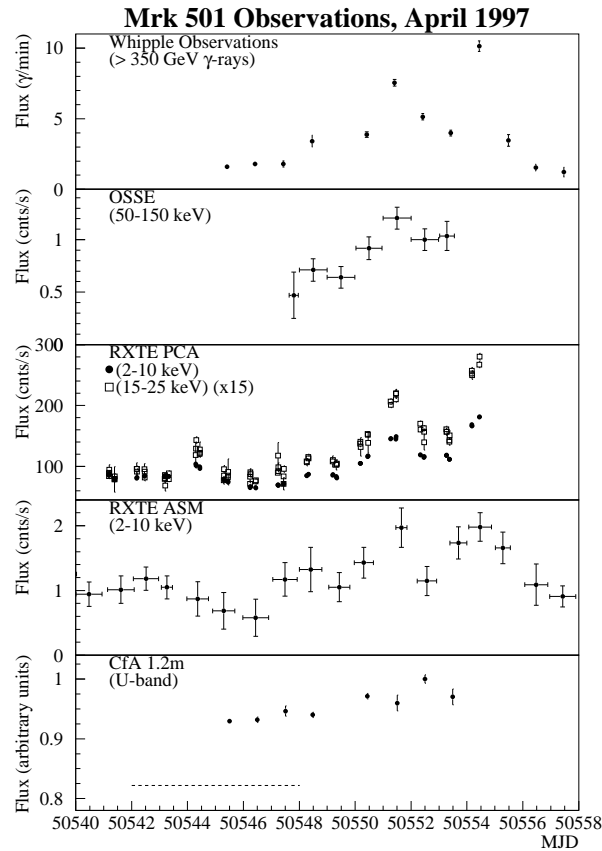


FIG. 1: *Left*: SED of Mrk 501 from contemporaneous and archival observations. *Right*: Multi-wavelength observations of Mrk 501; (a)  $\gamma$ -ray, (b) hard X-ray, (c) soft X-ray, (d) U-band optical light curves during the period 1997 April 2–20 (April 2 corresponds to MJD 50540). The dashed line in (d) indicates the optical flux in 1997 March. (from [20] and references therein.)

This figure is available as p42\_fig2.gif

FIG. 2: Simultaneous X-ray/ $\gamma$ -ray flare observed on March 19, 2001. The 2–10 keV X-ray light curve was obtained with the PCA detector on RXTE [22, 23]; data points are binned in roughly 4 minute intervals.

of the cosmic rays, but not the neutrinos) then it may be possible to produce a relatively large neutrino signal without overproducing the local cosmic ray flux [25]. While these models have a number of attractive features, there is some debate about whether they can provide a self-consistent description for the observations.

To overcome the threshold condition for pion production, protons must have energies in excess of  $10^{16}$  to  $10^{18}$  eV where abundant infrared photons can provide the target. Since the cross section for photo-pion production is relatively low, very high ambient photon densities are required to initiate the cascades. In this case, pair creation ( $\gamma\gamma \rightarrow e^+e^-$ ), which has a much higher cross-section, must be important. The proton cascade models may well have a significant problems explaining the emission from objects like Mkn 421/501 for this reason.

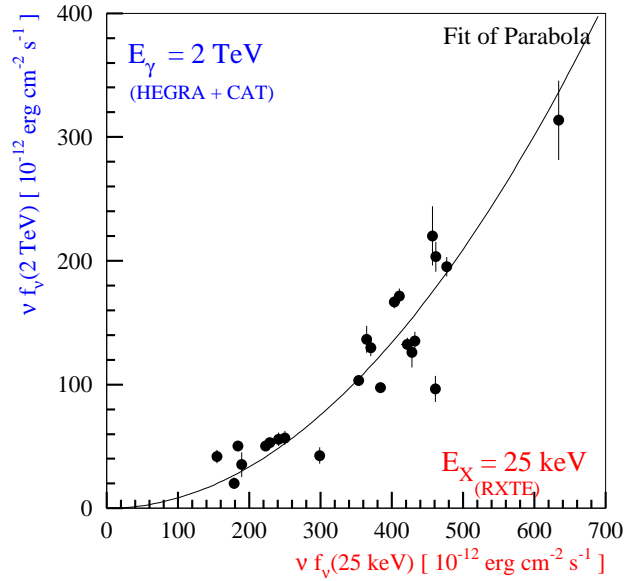


FIG. 3: Plot of TeV  $\gamma$ -ray flux versus X-ray flux measured with the HEGRA experiment during an intense flare of Mrk 501 (courtesy Henric Krawczynski).

In the PIC models [5] the proton-photon interaction occur with radio-IR photons in the jet. While a detailed analysis has not been published, Aharonian and others have pointed out that the required photon densities also imply large pair production optical depths, and may mean that the PIC models are not self-consistent. Models where the primary protons produce synchrotron radiation (and subsequent pair-cascades) may avoid this problem, but require even larger magnetic fields [26].

One advantage of the photon-pair cascade is that it produces a rather characteristic spectrum that does not depend sensitively on the model parameters. The detailed shape of this spectrum does not match some observations. Typically the spectra are too soft and overproduce X-rays, giving a spectrum that does not reproduce the strongly double-peaked spectrum observed. For the typical magnetic field values, the synchrotron spectrum is often too soft and lacks the spectral breaks that are observed.

For these hadronic models to account for the double-peaked spectrum, the radio to X-ray emission is most likely produced by primary shock-accelerated electrons, while the gamma-ray emission is produced by energetic secondary electrons from the cascade. There is no natural explanation for the correlated variability in the two spectral bands, or in the correlation in the X-ray and gamma-ray cutoff energy.

To reach these energies on a sufficiently short timescale, the gyroradius must be limited to a compact region in the jet, the inverse-Compton emission must be suppressed, and magnetic fields of up to 40 Gauss are required. The spectral variability seen in the X-ray waveband is consistent with much longer synchrotron cooling times than predicted by the hadronic models, and is quite consistent with magnetic fields of a 10 to 100 mGauss. This is the same value of the magnetic field derived by a completely independent method within the framework of the synchrotron inverse-Compton model.

The criticisms leveled at the electron models are that the magnetic fields are too small compared with the value required for magnetic collimation of the jets, and that the required electron energies are too large to be explained by shock acceleration. Moreover, electron injection into shocks is poorly understood since the electron gyroradius is small compared to the proton gyroradius and presumably to the width of the broadened shock front. However we know that electrons are accelerated to 100 TeV energies in supernovae shocks, regardless of the theoretical difficulties in accounting for this observation. As will be shown below, if one accepts relatively large Doppler factors, a self-consistent explanation for the VHE gamma-ray emission can be derived from leptonic models.

In the framework of either the EC or SSC models the  $\gamma$ -ray and X-ray data can be used to constrain the Doppler factor  $\delta$  (this is thought to be close to the bulk Lorentz factor of the jet for blazars) and magnetic field  $B$  in the emission regions of Mrk 421 and Mrk 501. The maximum  $\gamma$ -ray (IC) energy  $E_{C,\max}$  provides a lower limit on the maximum electron energy (with Lorentz factor  $\gamma_{e,\max}$ ) given by  $\delta\gamma_{e,\max} > E_{C,\max}/m_e c^2$ ; combining this with the measured cut-off energy of the synchrotron emission  $E_{\text{syn},\max}$  one obtains an upper limit on the

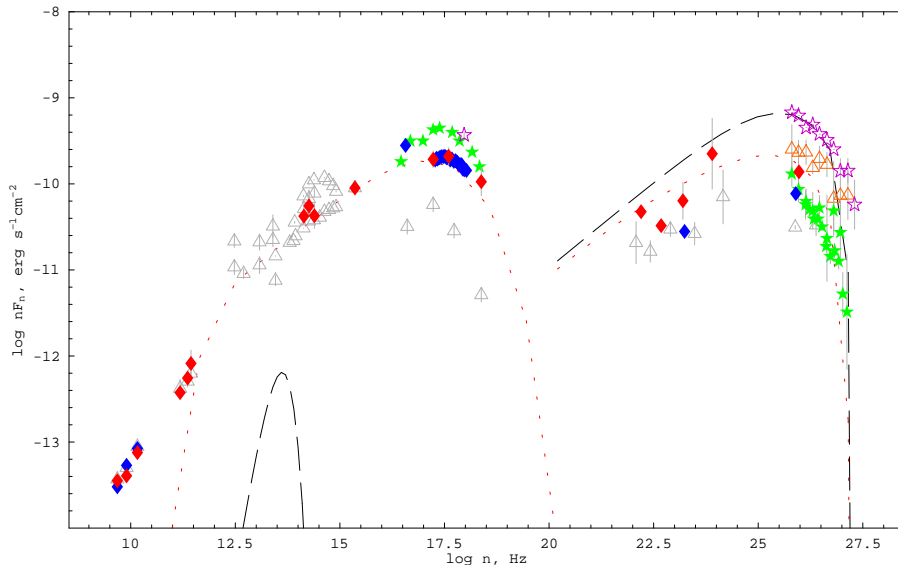


FIG. 4: Model fit to Mrk 421 SED with both an SSC and external Compton component[20]

magnetic field  $B \lesssim 2 \times 10^{-2} E_{\text{syn,max}} \delta E_{\text{C,max}}^{-2}$  (where  $E_{\text{C,max}}$  is in TeV). A lower limit on the magnetic field follows from the requirement that the electron cooling time,  $t_{\text{e,cool}} \approx 2 \times 10^8 \delta^{-1} \gamma_e^{-1} B^{-2}$  s, must be less than the observed flare decay timescale. These limits depend on the Doppler factor of the jet and in some cases cannot be satisfied unless  $\delta$  is significantly greater than unity [27, 28]. Typically, these arguments lead to predictions of  $\sim 100$  mGauss fields and Doppler factors  $\delta > 10$  to 40 for Mrk 421. Similar values for Mrk 501 but typically with a reduced lower limit on the Doppler factor. Model fits (that ignore the fact that the multiwavelength data are not truly time-resolved) give similar values for the Doppler factor and magnetic field strength. For example, a simple one-zone model fit for Mrk 421, shown in Fig. 4, only gives good fits for a Doppler factor approaching a value of  $\delta \approx 100$  (as shown) [20].

Doppler factors this large may present other problems. Radio observations of jets show radio components moving with velocities that imply bulk Lorentz factors  $\Gamma \lesssim 10$  further out in the jet. If the jet is decelerated by the inverse-Compton scattering, most of the energy would be used up before such extended radio lobes could form in apparent contradiction to observations.

Given the good progress to date, it appears that it will be possible to determine the dominant radiation processes in AGNs. After this first issue is resolved, further multiwavelength observations can address the more fundamental questions about the energetics of the central supermassive black hole, and the processes behind the formation of the relativistic jets. The very short variability timescales already observed with the Whipple instrument (15 minute doubling times for Markarian 421) hint that the gamma-ray observations may be probing very close to the central engine, beyond the reach of the highest resolution optical and radio telescopes.

## B. Gamma-Ray Bursts

Gamma-ray bursts (GRBs) were discovered by the Vela satellites in the late 1960's [29]. GRBs are bright flashes of hard X-rays and low energy gamma rays coming from random directions in the sky at random times. Until the launch of the CGRO in 1992 it was generally believed that GRBs were galactic phenomena associated with neutron stars. The BATSE instrument on-board the CGRO detected over 2000 GRBs and the observed spatial distribution was isotropic, with no evidence of an excess from the galactic plane. Thus GRBs were either cosmological or populated an extended galactic halo. In 1997 the BeppoSax satellite was launched. With a suite of hard X-ray detectors, this instrument has the ability to localize GRBs to within  $\sim 1$  minute of arc [30] (BATSE could localize GRBs to within  $\sim 5$  degrees). The increased angular resolution allowed conventional ground-based telescopes to search the error box without significant source confusion. The observation of emission and absorption lines from the host galaxies led to measurements of redshifts; some thirty years after their discovery the cosmological nature of gamma-ray bursts was determined. In Figure IIB we show the redshift distribution of those gamma-ray bursts where the redshift has been determined. The enormous energy output from GRBs, and transparency of the universe below 100 MeV makes GRBs visible across the universe. Thus gamma-ray

This figure is available as `p42_fig5.gif`

FIG. 5: The magnitude redshift distribution of gamma-ray bursts. Also shown on the plot is the magnitude vs. redshift relation for the observed type Ia supernovae.

bursts have the potential to probe the universe at very early times and to study the propagation of high-energy photons over cosmological distances.

To use GRBs as cosmological probes it is necessary to understand their underlying mechanism. While GRBs may never be standard candles on par with the now famous Type-IA supernovae, there has been great progress made in the last five years in understanding GRBs. While we still do not know what the underlying energy source is, we are beginning to understand the environment that creates the observed high-energy photons.

The large distances to GRBs implies that the energy released is  $\sim 10^{50-54}$  ergs, depending on the amount of beaming at the source. While the origin of the initial explosion is unknown, the subsequent emission is well described by the relativistic fireball model. In this model shells of material expand relativistically into the interstellar medium. The complex gamma-ray light-curves of the prompt radiation arises from shocks formed as faster and slower shells of material interact. A termination shock is also formed as the expanding shells of material interact with the material surrounding the GRB progenitor. In this model the observed afterglows (x-ray, optical, and radio) arise from the synchrotron radiation of shock accelerated electrons.

The afterglow emission can be used to determine the geometry of the source. Since the shell is expanding relativistically, the radiation (emitted isotropically in the bulk frame) is beamed into a cone with opening angle  $\Gamma^{-1}$  (the bulk Lorentz factor of the material in the shell). Thus at early times, only a small portion of the emitting surface is visible and one cannot distinguish between isotropic and beamed (jet-like) emission. However, as the shell expands it sweeps up material and  $\Gamma$  decreases. If the emission is not isotropic the beaming angle ( $\Gamma^{-1}$ ) will eventually become larger than the opening angle of the jet. At this point one should observe a break in the light curve (luminosity versus time) of the afterglow. This distinctive feature has been observed in 15 GRBs. By measuring the temporal breaks in GRBs of known redshift Frail et al., [31] have measured the jet opening angles of 15 gamma-ray bursts (with some assumptions about the emission region: the jet is uniform across its face, the electron distribution in the shock is a power law, the afterglow radiation is due to synchrotron emission and inverse Compton scattering). If one integrates the observed luminosity over the inferred jet opening angle one can determine the intrinsic luminosity of each GRB. Surprisingly, Frail et al., conclude that the intrinsic luminosities of the observed gamma-ray bursts are peaked around  $5 \times 10^{50}$  ergs with a spread of roughly a factor of six. Thus the observed variation in luminosity (a factor of  $\sim 500$ ) may be mainly due to the variation in the jet opening angle. Note that this conclusion applies only to the “long” GRBs, as these are the only GRBs for which optical counterparts have been observed.

With a similar goal, to reduce the wide divergence in the observational properties of GRBs, Norris [32] has found a correlation between energy dependent time lags and the observed burst luminosity. Three things occur as one moves from high energy photons to low energy photons. The pulse profiles widen and become asymmetric, and the centroid of the pulse shifts to later times. The time lag is defined as the shift in the centroid of the pulse profile in the different energy channels of the BATSE instrument. In Figure IIB we show the observed luminosity (assuming isotropic emission) versus the time lag observed between two energy channels on the BATSE experiment. (Channel 1 corresponds to photons with energies between 25–50 keV and channel 3 to 100–300 keV photons.) The line is the function,  $L_{53} = 1.1 \times (\tau_{lag}/0.01s)^{-1.15}$ , where  $L_{53}$  is the luminosity in units of  $10^{53}$  ergs. It may be that the time lag is dependent upon the jet opening angle for reasons that are not yet understood and this observed correlation is simply an way of parameterizing the relationship observed by Frail et al.

As discussed above, gamma-ray observations of AGNs revealed a new spectral component due to inverse-Compton emission, distinct from the synchrotron emission observed in the radio to X-ray wavebands. This observation resulted in an independent constraint on the electron energy that allowed a determination of the magnetic fields, electron densities, and bulk Lorentz factors in the sources. While AGNs are quite different for GRBs, the non-thermal radiation mechanisms may be quite similar, and we might expect similar progress to follow from high energy gamma-ray measurements.

At higher energies less is known about GRBs. The EGRET instrument covered the energy range from 100 MeV to a few tens of GeV. EGRET detected several GRBs at high energy (HE  $E > 100$  MeV). From EGRET



This figure is available as p42\_fig6.gif

FIG. 6: Observed GRB luminosity, assuming isotropic emission vs. observed lag between high and low energy photons in the BATSE instrument. Channel 1 includes photons with energies between 25 and 50 keV and channel 3 includes photons between 100–300 keV.

observations we know that the energy spectrum is a power law that extends to high energies  $\sim$ GeV. However, dead-time in the EGRET spark chambers compromised the ability of EGRET to measure light curves and spectra.

The high energy spectrum is of inherent interest in understanding the environment of the GRB. Observations above MeV energies provide important constraints on the Doppler factor. Without a large Doppler factor, photon-photon pair production interactions would cut off the photon spectrum. The highest energy photon observed from a GRB was seen by EGRET. They detected an 18 GeV photon from a GRB [33] that arrived roughly 90 minutes after the lower energy photons (25–150 keV observed by Ulysses). There has also been tantalizing evidence of even higher energy photons from gamma-ray bursts. The Milagrito detector, a ground-based gamma-ray telescope, observed an excess of events (18 observed on a background of 3.46 events) in spatial and temporal coincidence with GRB 970417a. However, due to the poor localization of the BATSE detection and the large number of bursts examined (54), the detection is marginal ( $\sim 3\sigma$ ). If the observed excess is not due to a statistical fluctuation the implied photon energies from the burst are  $\gtrsim 200$  GeV.

There are new instruments both running and planned that should greatly increase the sample of high-energy photons seen from gamma-ray bursts. Figure II B shows the sensitivities of EGRET, Milagro, and GLAST. The sensitivity plotted for Milagro assumes that the source spectrum continues to TeV energies and is unaffected by intergalactic absorption (GRBs with a redshift beyond  $\sim 0.3$ – $0.5$  should not be visible to Milagro).

VERITAS will also have sensitivity to GRBs if a TeV afterglow persists for a few minutes and the burst has been localized to within  $\sim 1$  degree, so the telescopes can slew to the source. In Figure II B we show power-law extrapolations of two EGRET detected GRBs using the measured spectral indices. Since no redshifts were available for these sources, for illustration we calculate the effect of infrared absorption on one source assuming a moderately large redshift ( $Z = 1$ ) and for the other source assuming a redshift closer to the minimum value determined for a GRB.

All of these instruments will have vastly increased sensitivity to the high energy spectrum of gamma-ray bursts, and we should be able to better understand the environments (bulk Lorentz factor, magnetic fields, and particle densities) around the GRB.

Wide field instruments like GLAST and Milagro have natural advantages for detecting GRBs. While Cherenkov detectors suffer from a small field of view, and small limited duty cycle (about 10% corresponding to dark moonless night) compared with MILAGRO and GLAST, their relatively large effective areas above  $\sim 50$  GeV should prove important for a small fraction of GRBs. The sensitivity of air Cherenkov telescopes is good enough that even for a source at a redshift of  $z \approx 1$ , with several e-foldings of attenuation, a strong detection could be possible. If the VHE emission persists long enough to be detected, the huge effective area of ground-based telescopes such as VERITAS would provide as many as  $10^4$  times the number of detected photons above 100 GeV as space-based experiments, greatly enhancing the spectral reach of GLAST.

### C. Search for Dark Matter

One of the most exciting prospects for future gamma-ray experiments is the possibility of detecting the unambiguous signature of cold dark matter in the galaxy through the annihilation of these particles to a gamma-ray line. However, as most will have surmised from this Snowmass workshop, the standard Cosmological model has been in a dramatic state of upheaval in recent years. For this reason it is worth first revisiting the case for cold dark matter, then looking in detail at the prospects for a gamma-ray detection.

Over the last couple of years our knowledge of the inventory of matter and energy in the universe has improved dramatically. Astrophysical measurements from disparate experiments are now converging and a standard cosmological model is emerging. The most significant new data come from recent measurements

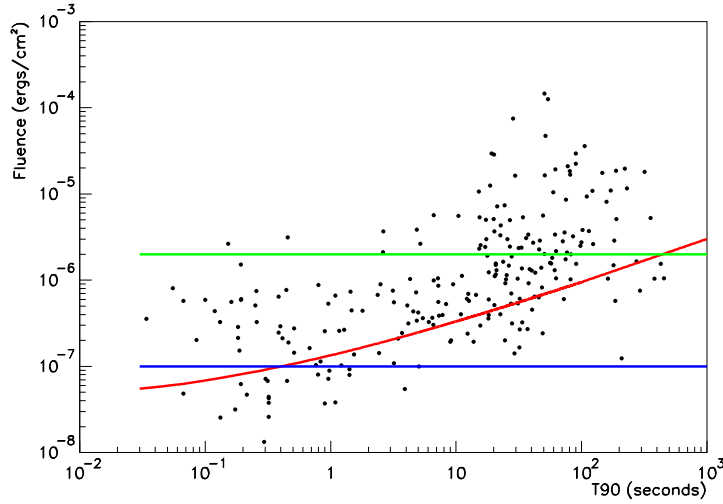


FIG. 7: Fluence sensitivity of EGRET (green line) Milagro (red) and GLAST (blue) to GRBs as a function of burst duration. The data points show the distribution of fluence and duration seen by the BATSE instrument.

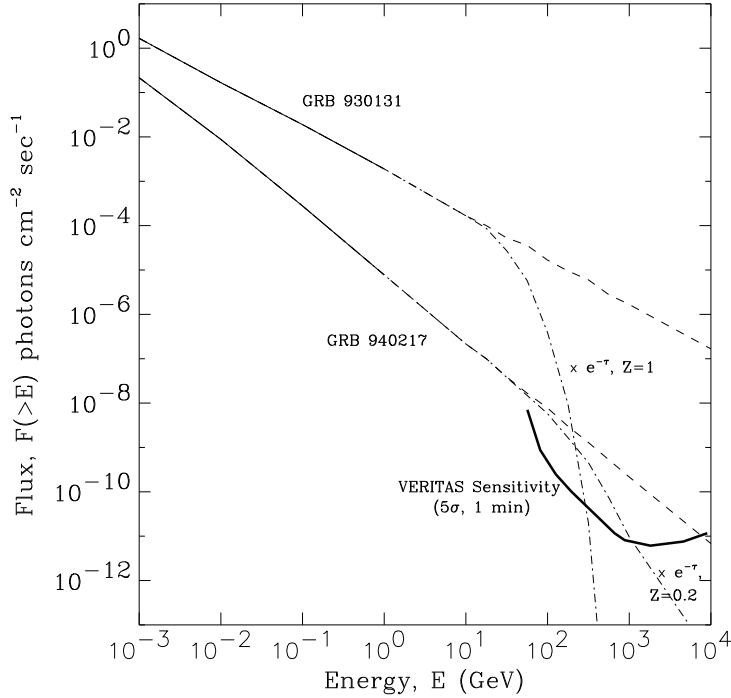


FIG. 8: Sensitivity of VERITAS to two hypothetical bursts extrapolated from EGRET detections.

of the cosmic microwave background radiation (CMBR) and measurements of the Hubble flow using distant supernovae.

Temperature fluctuations in the CMBR trace the matter distribution at the time that electrons and protons combined to form atoms, and matter and radiation decoupled. Measurements of the power spectrum of the fluctuations tell us that, the density of the universe is close to the critical density ( $\Omega_{\text{tot}} \approx 1$ ) and that matter, both luminous and dark, makes up at most 30% of the total.

Type IA supernovae have been detected out to a redshift of 1.7. Despite the intuitive idea that gravity should be causing the universal expansion to slow down, the luminosity redshift relationship shows evidence for a slower expansion in the past than in the present. This *acceleration* can only be explained by a form of dark energy

with a strange equation of state that results in a net repulsive force, where the total dark energy density is given by  $\Omega_\Lambda \approx 0.7$ . How does this discovery affect our expectations about the matter density of the universe?

It is now well established from the observation of galactic rotation curves that our galaxy is comprised of a dark halo of density  $\Omega_{\text{halo}} > 0.1$  which extends well beyond the distribution of visible matter ( $\Omega$  is defined as the ratio of the density  $\rho$  to the critical density  $\rho_{\text{crit}}$  for which the universe is flat). Large scale motions of galaxies on the scale of clusters and superclusters indicate a still higher value of  $\Omega \gtrsim 0.2 - 0.3$  (in good agreement with a  $\Omega_{\text{total}} - \Omega_\Lambda$ ). However, an inventory of the stars shows that only about 10% of this total is in the form of luminous matter. Much effort has gone into determining the nature of this unseen, or dark, matter.

Until recently, the best handle on the amount of ordinary (baryonic) matter came not from starlight, but from measurements of the primordial abundances of deuterium,  $^3\text{He}$ ,  $^4\text{He}$  and  $^7\text{Li}$ . Detailed calculations of nucleosynthesis in the very early universe require that the total amount of matter in the form of baryons is  $0.008 \lesssim \Omega_{\text{baryon}} h^2 \lesssim 0.024$ , or conservatively  $\Omega_{\text{baryon}} \lesssim 0.1$ . More recently, the position and intensity of the second acoustic peak in the CMBR has been used to independently determine the total baryon density. This peak in the CMBR power spectrum is determined by the balance between the restoring force of photon pressure on baryons and the gravitational force, giving a new measure of the baryonic density of the universe. The two measurements agree amazingly well, providing further support for a standard cosmology, but revealing a large component of the matter density of the universe that is non-baryonic and is distinct from the *dark energy*.

Moreover, if most of the matter in the universe is non-baryonic it is reasonable to assume that much of the matter comprising our own galactic halo is non-baryonic as well. The origin of structure relatively early in the history of the universe strongly favors cold dark matter (matter that was relativistic at the time of decoupling). In the hierarchical CDM structure formation models, the cool dissipationless gas of dark matter first forms small structures that are the building blocks of successively larger structures. These eventually form the gravitational potential wells into which baryonic matter fall to form the observed galaxies.

The detection of this dark matter has been a priority of the physics community over the past decade; the astrophysical motivation for cold dark matter is not changed by the recent discoveries. The composition of this dark matter is unknown, but astrophysical data suggest that any weakly interacting massive particle (WIMP) could provide a natural explanation. The argument for weakly interacting particles goes as follows [34]:

Initially the universe was very hot and dense and all particle species were in thermal equilibrium. As the universe expanded, particle species initially followed their equilibrium value until the interaction rate  $\Gamma_A = n_\chi \langle \sigma_A v \rangle$  fell below the Hubble expansion rate  $H$ , resulting in decoupling or *freeze-out*. For stable particles, the number density per co-moving volume after freeze-out is constant. From this freeze-out condition,  $\Gamma = n_\chi \langle \sigma_A v \rangle = H$ , it is apparent that the larger the value of the thermally averaged product of the annihilation cross section and the relative velocity  $\langle \sigma_A v \rangle$ , the longer the particle stays in equilibrium, and the more it is Boltzmann suppressed before freeze-out.

A quantitative solution of the Boltzmann equation yields the present mass density in units of the critical density:

$$\Omega_\chi h^2 \approx \frac{3 \times 10^{-27} \text{cm}^3 \text{sec}^{-1}}{\langle \sigma_A v \rangle} . \quad (1)$$

For a particle of mass  $m_\chi$  with weak-scale interactions,

$$\langle \sigma_A v \rangle \sim \left( \frac{m_\chi}{100 \text{ GeV}} \right)^2 10^{-25} \text{cm}^3 \text{sec}^{-1} , \quad (2)$$

which is very close to the value required to provide  $\Omega = 0.3$ . This means that if there exists a new stable massive particle with weak-scale interactions (i.e., a WIMP), it is a natural candidate for the dark matter.

Perhaps the best motivated of these particles is the neutralino [35], the lightest, stable supersymmetric particle predicted by the supersymmetric extension of the standard model (see Jungman, Kamionkowski and Greist [34] for a comprehensive discussion of neutralino dark matter and the prospects for detection). Calculations of the relic abundance and mass of the neutralino suggest that they could be the dark matter if their mass is below a few TeV.

At this meeting J. Ellis and others presented updated calculations of relic abundances taking into account co-annihilations and resonances in the annihilation cross-section in the early universe. These effects destroy the simple one-to-one relationship between the two-photon annihilation cross section in the present universe and the total annihilation cross section at the time of decoupling, and alter our expectations about the cosmologically viable range of parameter space. Without fine tuning, the likely mass range of the neutralino is  $\sim 100 \text{ GeV}$  to  $\sim 1 \text{ TeV}$ . However, Higgsino-like neutralinos with masses up to 8 TeV are possible without violating the upper limit  $\Omega_{\text{CDM}} < 0.3$ . (These models are considered somewhat distasteful as they require fine-tuning and are viewed to be less satisfactory in solving the hierarchy problem.) Of course if the anomalous muon magnetic moment

$g - 2$  result stands, then the limit changes. If the DAMA observation of an annual modulation in the detector signal is valid, the neutralino may have already been discovered (see the report of P4.6 in these proceedings). The implications of the  $g - 2$  measurement are made somewhat murky by theoretical uncertainties in QCD, and the DAMA direct detection results may be undermined by systematic errors in understanding background rates in the detectors.

If the dark matter in the galactic halo is comprised of cold, weakly interacting particles (e.g., neutralinos) then these particles should annihilate with each other giving a potentially observable signal in a number of different annihilation channels. The annihilation rate is proportional to the thermally averaged product of the annihilation cross section and relative velocity, and to the square of the dark matter halo density.

Annihilation will result in direct or cascade production of protons, antiprotons, electrons, positrons, neutrinos and gamma rays that can stand out above the corresponding cosmic-ray backgrounds. Such *indirect* detection techniques are sensitive to astrophysical uncertainties that enter into an estimation of the halo density and the backgrounds, but nonetheless can complement direct and accelerator searches.

For a reasonable fraction of parameter space (covering varying values for the neutralino mass and annihilation cross-section) the local flux of antiprotons and positrons can give a signal detectable by the current generation of cosmic-ray experiments. The only astrophysical uncertainty that enters into the calculated flux comes from the relatively well established local halo density. Unfortunately, the signal has proven very difficult to discriminate from other cosmic-ray backgrounds, especially in the case of the anti-proton flux [36]. The recent measurement of the cosmic-ray positron fraction by the HEAT experiment [37, 38], may reveal a hint of an excess from the annihilation signal, but uncertainties in backgrounds again make it very difficult to draw a definitive conclusion [39].

A high energy neutrino signal could also be observed and has provided an impetus for proposals to build  $\sim\text{km}^3$  neutrino detectors. The gravitational field of the Earth and Sun are expected to enhance the local density of neutralinos in the core of these objects, thereby substantially increasing the annihilation rate. The emergent high energy neutrinos would offer a tell-tail signature, since no standard astrophysical process could explain GeV to TeV neutrinos emerging from the centers of such garden-variety celestial bodies! The predicted signal depends on the local halo density and the capture cross-section, but is thought to be reasonably well understood. Future detectors such as ICECUBE will be sensitive to a sizable fraction of the particle physics parameter space.

Annihilation to charged particles will result in cascade emission of continuum gamma rays, and direct annihilation to two gamma rays (or a  $Z$  and a gamma) will result in two nearly monochromatic lines at roughly the neutralino mass. While the monochromatic line offers a smoking-gun signature for the dark matter, an observable flux is generally only expected in the direction of the galactic center where the dark matter density peaks. The predicted flux is much more sensitive to the detailed astrophysical model for the halo than the positron, antiproton or neutrino measurements.

Recent N-body simulations of cold-dark-matter structure formation indicate the possibility of cusps in the central density profile. This has resulted in considerable optimism, since if true it would mean that the gamma-ray detection channel could potentially provide access to essentially the *entire* parameter space, a smoking-gun signature in the form of a narrow annihilation line that could not be confused with any astrophysical background, a measurement of the neutralino mass, and a measurement of the dark matter halo profile.

The detectability of a gamma-ray signal from neutralino annihilation is extremely sensitive to the density profile of dark matter within the galaxy [40]. Numerical simulations of the growth of structure in the universe suggest that the mass density of dark matter halos may increase as a power law towards the centers of galaxies. The existence of these density cusps is controversial: there is some observational evidence against such dark matter cusps [41, 42, 43], other evidence may be consistent with them [44, 45]. If there is a density cusp at the galactic center the neutralino annihilation rate may be large enough so that the resulting rays would be detectable above the background by atmospheric Cherenkov detectors and GLAST[40].

In the halo, the number of gamma rays produced per unit volume per unit time is given by the source function

$$q_\gamma = 2\langle\sigma_{\chi\chi\rightarrow\gamma\gamma}v\rangle n_\chi^2 \quad . \quad (3)$$

The observed flux is obtained by integrating this source function along the line of sight. If we observe at an angle  $\theta$  with respect to the direction of the galactic center, into an infinitesimal solid angle  $d\Omega$ , then summing over the differential elements of volume  $l^2 dl d\Omega$  along the line of sight gives

$$\frac{d\phi_\gamma}{d\Omega}(\theta) = \int_0^\infty q_\gamma(r) \frac{1}{4\pi l^2} l^2 dl \quad . \quad (4)$$

This can be rewritten as

$$\frac{d\phi_\gamma}{d\Omega}(\theta) = 3.7 \times 10^{-13} \left( \frac{\langle\sigma_{\chi\chi\rightarrow\gamma\gamma}v\rangle}{10^{-29}\text{cm}^3\text{s}^{-1}} \right) \left( \frac{100\text{ GeV}}{m_\chi} \right)^2 I(\theta) \text{ cm}^{-2}\text{sec}^{-1}\text{sr}^{-1} \quad , \quad (5)$$

This figure is available as p42\_fig9.gif

FIG. 9: (a) Value of the line of sight integral  $I(\theta)$  for four different halo models (b) relative signal to background ratios for these models as a function of the angular acceptance interval given by the solid angle  $\omega$  about the direction  $\theta = 0^\circ$ . Also shown are three models where the cusp has a constant density core.

where the dimensionless line of sight integral  $I(\theta)$  has been normalized using our galactocentric distance  $R_\odot \approx 8.5$  kpc and the local halo density  $\rho_\odot \approx 0.3$  GeV cm $^{-3}$  (as determined from measurements of the galactic rotation curve) and is given by:

$$I(\theta) = (\rho_\odot^2 R_\odot)^{-1} \int_0^\infty \rho^2(r(l, \theta)) dl \quad (6)$$

where

$$r(l, \theta) = \sqrt{l^2 + R_\odot^2 - 2lR_\odot \cos \theta} \quad . \quad (7)$$

Figure 9 shows the line of sight integral  $I(\theta)$  calculated for a number of different halo models, variants of typical centrally-peaked profiles (without spikes) as well as models with constant density cores of varying radius (assuming that the central halo was disrupted [46]). For comparison, we show the more traditional (but perhaps less well motivated) isothermal halo that lacks the central density enhancement required to give an appreciable annihilation signal. Also shown in Figure 9 is the relative signal to background ratio ( $S/\sqrt{B}$ ) for observations centered on the galactic center as a function of the angular acceptance window given by the solid angle  $\omega$ . This assumes that the observations are dominated by an isotropic background so that  $\sqrt{B} \propto \omega^{1/2}$ . All halo models have been renormalized so that the total mass inside the solar radius  $R_\odot$  is the same as that of the standard isothermal halo, thus matching the observed galactic rotation curve at large distances from the galactic center. The signal is obtained by integrating  $I(\theta)$  over a region of solid angle  $\omega$  centered on the galactic center. Thus

$$S/\sqrt{B} = \omega^{-1/2} \int_\omega I(\theta) 2\pi \theta d\theta \quad . \quad (8)$$

Combining this astrophysical input with the particle physics calculation of the annihilation cross-section for different supersymmetric models one obtains the results shown in Fig. 10 [40]. Here the predicted annihilation flux for the NFW halo are shown as a function the neutralino mass. Only models satisfying the cosmological and accelerator constraints are shown. Also shown is the sensitivity of GLAST and ground based instruments to the line flux. Since the resulting signal to noise ratio shows a strong dependence on the detailed halo model, a comparison of the SNR for the NFW halo and for other halo models (as shown in Fig. 9) can be used to slide the sensitivity curves up or down with respect to the model points; for some halo models with relatively steep central cusps almost the entire parameter space is accessible. If the observed bump in the HEAT positron spectrum is really an indication of neutralino annihilation, then the allowed parameter space is as shown in Fig. 11 [39]. Future ground arrays such as MAGIC, VERITAS and HESS would be sensitive to almost the entire parameter space for halo models with a modest cusp.

The issue of the existence of WIMP cusps is exacerbated by an additional, possibly strong, concentration of dark matter around the black hole at the galactic center [47, 48]. (Traditionally, this additional concentration follows a power law in density and would be called a cusp, but, to distinguish it from the halo density cusp of N-body simulations, it has been referred to as a spike. We define any power law density profile with a spectrum steeper than  $\sim r^{-2}$  around the black hole as a steep spike, and any shallower power law profile as a shallow spike.) The spike could originate during the gradual (adiabatic) growth of the central black hole as dark matter is trapped and the gravitational potential gets deeper. A similar phenomenon occurs with stars (which also act as a dissipationless gas) and is believed to be the cause of the observed stellar concentrations around the central black holes of elliptical galaxies and bulges of spiral galaxies.

The dark matter spike at the galactic center may be shallow or steep according to the phase space density of dark matter at the time the black hole formed [48], depending on whether the center of dark matter distribution and black hole were coincident, and depending on whether the black hole was formed adiabatically or through

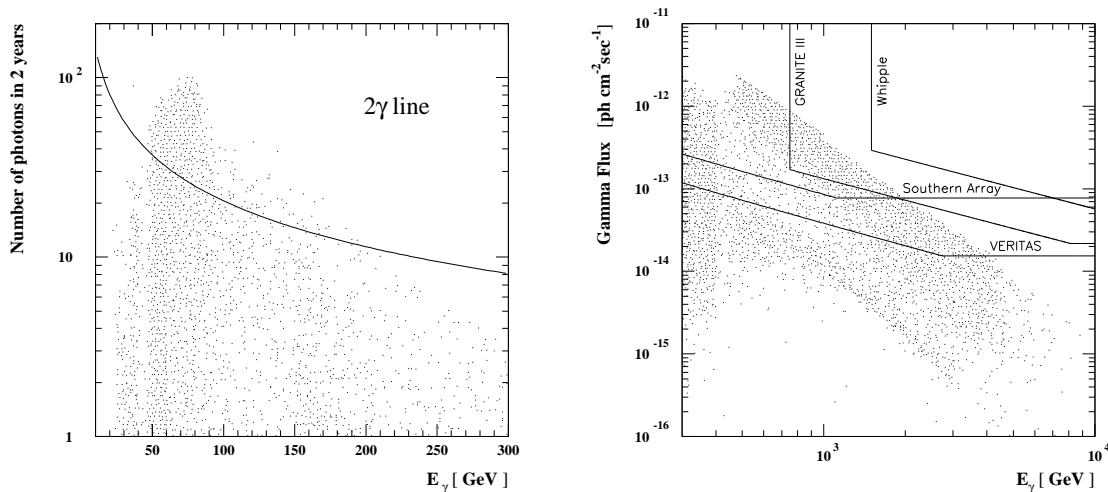


FIG. 10: Predicted gamma-ray line flux for allowed supersymmetric parameter space assuming a NFW halo [40]. *Left*: GLAST sensitivity based on preliminary specifications of the wide-field calorimeter mode [40]. *Right*: The expected sensitivity for a five year exposure at large zenith angles with VERITAS or HESS, and small zenith angle observations (made for the same duration) from the southern hemisphere.

This figure is available as p42\_fig11.gif

FIG. 11: If the observed excess in the positron fraction measured with the HEAT experiment is correct, then GLAST and ACTs might be expected to verify the signal. Above is shown the predicted gamma-ray line flux, and sensitivity of one of the ACT detectors currently under construction. The flux from both high galactic latitude and from the galactic center is indicated assuming a conservative halo model, and showing only models that pass constraints from fitting the positron data (Adapted from [39]).

impulsive mergers [46]. At this meeting Merritt described simulations of baryonic and dark matter structure formation at the centers of galaxies with massive black holes. His simulations show that the stellar and dark matter spikes could be destroyed by mergers, explaining why stellar spikes are only observed in a subset of galaxies.

Gondolo and Silk [48] considered the case of adiabatic growth of a black hole coincident with the center of the dark matter distribution. If there was a high density of slow dark matter particles, and a black hole would form gradually at the center of such a halo, the spike would be steep. If the initial distribution was isothermal, the dark matter spike would be shallow, leading to a dark halo with a central core. Figure 12 illustrates steep and shallow spikes for four models of a WIMP galactic halo. Two of the models shown, the canonical model [49] (marked “can”) and the model by Persic, Salucci, and Stel [50] (marked “PS”), have a core. The other two models, that by Navarro, Frenk, and White [51] (marked “NFW”) and that by Moore et al. [52] (marked “M&”), have a cusp. Both types of models have a central spike, models with a cusp having a steeper spike. The density in the spike follows essentially a power law, except when it becomes so high that the WIMP annihilation timescale is comparable to the age of the black hole. In this case, the density remains constant (“annihilation plateau”). The spike’s innermost radius occurs where the WIMPs are captured by the black hole.

The steepness of the spike is crucial when considering the annihilation of WIMPs in the spike: while a shallow spike is undetectable, a steep spike may give rise to a detectable signal in high-energy neutrinos and gamma-rays [48]. Furthermore, with a steep spike, electrons and positrons generated in WIMP annihilation

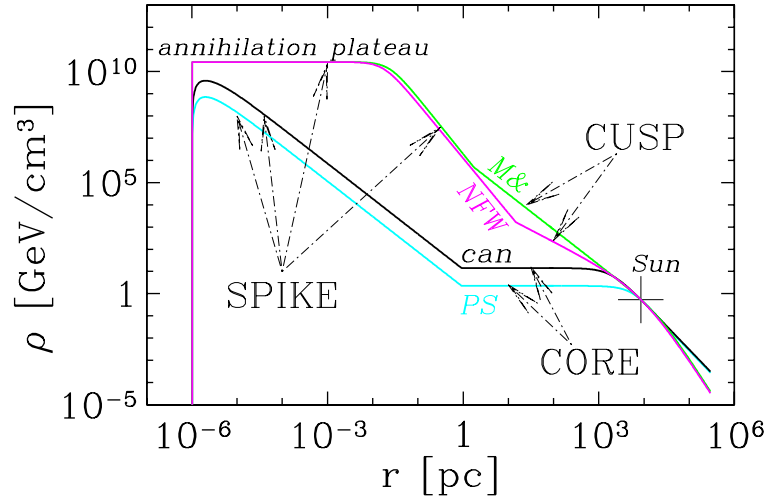


FIG. 12: Dark matter density as a function of distance from the galactic center, showing spikes, cusps, and cores. Four density models are shown: canonical (“can”), Persic–Salucci (“PS”), Navarro–Frenk–White (“NFW”) and Moore-et-al. (“M&”). The models are normalized to the same rotation velocity and the same density at the Sun’s position (marked by a cross).

This figure is available as p42\_fig13.gif

FIG. 13: EGRET observations of the galactic center region from Mayer-Hasselwander et al. (1997). (a) background-subtracted, smoothed  $E_\gamma > 1\text{ GeV}$  count map, (b) 300 MeV – 1 GeV map.

may produce synchrotron emission well in excess of the observations [47], ruling out WIMP dark matter at the galactic center.

Gondolo argues that the most natural way to avoid a steep spike is not to have a halo cusp in the first place, in line with the observations against the existence of halo cusps [41, 42, 43]. Indeed a series of suggestions to eliminate halo cusps have been proposed, some of which do not dismiss WIMP dark matter [53, 54, 55]. Without a halo cusp, however, the prospect of detecting WIMP dark matter through gamma-ray emission is bleak.

However, this conclusion seems to have some significant caveats. It is possible to have a halo cusp without a steep central spike if the black hole did not form at the center of the dark halo or if the present black hole is the result of merging two or more previous black holes [46, 56]. It is still an open question if these scenarios are compatible with the observed existence of a steep *stellar* spike around the black hole at the galactic center [57]. Until the theoretical uncertainties are resolved any non-detections of WIMP annihilation lines give poor constraints on the existence of WIMPs. However, the possibility of large density enhancements at the galactic center provide the potential for discovery, and mean that gamma-ray observations may provide one of the few methods for which the entire allowed parameter space is accessible. Of course a detection of gamma rays from WIMP annihilations would be enormously important since it could provide a smoking-gun signature for nonbaryonic dark matter, provide indirect evidence for supersymmetry, would provide a measurement of the dark matter mass, and would also provide information about the dark matter profile that would serve as a sensitive test of our theoretical understanding of structure formation.

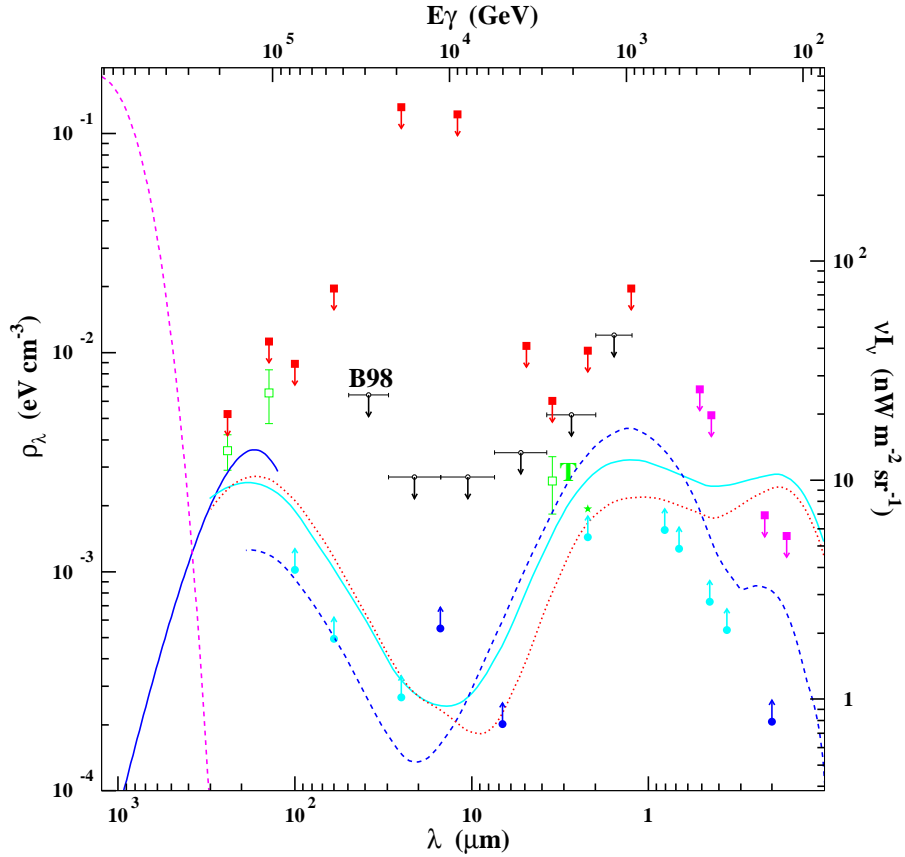


FIG. 14: Spectrum of the extragalactic background light with initial *measurements* by DIRBE, upper limits by Whipple [60] and lower limits from K-band galaxy counts (adapted from [61]).

To date there have been some modest searches for the annihilation line with only upper limits on the flux [58]. However, it is interesting to note that the observed GeV flux at the galactic center is consistent with the continuum flux predicted in some of the more optimistic halo models. While this does not constitute a detection and may well be associated with some other gamma-ray source, there is certainly room for the continuum component [59]. Clearly the detection of an annihilation line will be required to obtain an unambiguous result.

#### D. The Cosmic Infrared Background

Gamma-rays also can be used as probes of the the extragalactic background light (EBL), the relic starlight that fills the universe. The diffuse infrared background light contains contributions from redshifted starlight, starlight that has been scattered by dust, and any of a number of processes in the history of the universe that have pumped significant amounts of energy into the infrared (IR) to energy band. A large contribution to this primordial radiation field comes from the era of galaxy formation, when most of the star formation occurred. Direct measurement of the characteristics of this radiation are difficult due to the dominance of local galactic IR sources.

TeV gamma-ray astronomy provides a means to study the IR background free of such complications by looking for modifications to high energy gamma-ray spectra. Gamma rays from distant AGN interact with this background field via the process  $\gamma\gamma \rightarrow e^+e^-$  [17, 18]. Since this is a resonant process, with a large cross section when the center-of-mass energy of the two photons is equal to twice the electron mass, the spectra of distant AGNs becomes distorted. The quantitative effect on the AGN spectrum depends on the spectrum of the EBL.

Measurements of the spectra of the TeV sources Mrk 421 and Mrk 501 have been used to set an upper limit on the density of extragalactic background photons (under the assumption that the intrinsic source spectra do not become harder or rise exponentially above a few hundred GeV). The resulting limits are more than an order of magnitude more restrictive than direct observations in the 0.025-0.3 eV regime [60] and are shown in Figure 14. Also shown in the figure are direct measurements by DIRBE and lower limits come from K-band galaxy



counts. Model curves from [62] show sensitivity to the history of star formation (e.g., CHDM vs. SCDM) in the 1-10 $\mu\text{m}$  regime and sensitivity to the initial mass function and re-radiation by dust in the interval ( $\lambda \lesssim 1 \mu\text{m}$  and  $\lambda \gtrsim 10 \mu\text{m}$ ).

Combining the numerous AGN spectra measured with GLAST with the ground-based experiments one will obtain the detailed spectra of a large number of sources required to disentangle the intrinsic absorption from the intergalactic absorption, providing a measurement of the EBL. This is an important example where space and ground-based instruments acting together are much more powerful than either instrument acting alone. To make this measurement in the infrared portion of the spectrum, it is critical that the GLAST measurements of the largely unabsorbed spectra at lower energies be complemented by measurements with ground-based telescopes. Above 50 to 100 GeV, the huge effective area of ground-based experiments will be required to overcome the counting-statistics limitation of satellite experiments and measure the spectral cut-offs. The overlap with GLAST will be critical to calibrate the ground-based instruments. Furthermore, while the ground-based telescopes may make the most sensitive measurements of spectral cutoffs of some sources, the GLAST spectral measurements over almost 3 orders of magnitude (from 100 MeV to 100 GeV) will provide information about the source spectrum essential for normalizing the VHE measurements and making reliable constraints.

### E. Primordial Black Holes

Stephen Hawking first postulated that black holes might in fact not be completely black [63]. Hawking showed that a black hole has an effective temperature that is related to the mass of the hole by  $T = 10^{13}/M$  GeV (where  $M$  is given in grams). Since the emission is nearly thermal the luminosity of the black hole is given by  $\mathcal{L} \propto 1/M^2$ . As the hole radiates energy, its mass decreases, it gets hotter and radiates more rapidly. This runaway process leads to the eventual evaporation of the hole. Black holes formed during the early universe with a mass  $\sim 10^{15}$  grams would be evaporating now ( $t \approx 10^{10}(M/10^{15})^3$  yr). The evolution of the luminosity of a black hole depends upon the number of degrees of freedom available. As the temperature rises and heavier particles can be created the luminosity increases. In principle one can probe the particle spectrum up to the Planck scale by measuring the luminosity evolution of an evaporating black hole. There is further interest in the Hawking radiation because it relies on the application of relativistic quantum field theory in the presence of the strong field limit of gravity, a situation that could potentially be observed.

To set the scale from fundamental physics, we note that the spontaneously broken gauge symmetry in the electroweak sector of the standard model gets restored in a phase transition or rapid crossover at a temperature near 100 GeV. The fact that temperatures of the latter order of magnitude will never be achieved in a terrestrial experiment should motivate us to study the fate of microscopic black holes during the final few days of their lives when their temperatures have risen to 100 GeV and above. The fact that microscopic black holes have not yet been observed should not be viewed as a deterrent, but rather as a challenge for the new millennium. Lacking a firm cosmological prediction for the relic abundance, we address the question: What would be the observable signal?

When the Hawking temperature exceeds a few hundred MeV we should expect that jets of quarks and gluons are emitted which then fragment into hadrons, an idea first proposed by MacGibbon, Webber and Carr [64]. Subsequently Heckler [65, 66] argued that at sufficiently high temperatures the emitted quarks and gluons are so densely packed outside of the event horizon that they do not fragment into hadrons in a vacuum but in something more akin to a quark-gluon plasma. He also argued that QED bremsstrahlung and pair production were sufficient to lead to a thermalized QED plasma when  $T_H$  exceeded 45 GeV. A more quantitative treatment of the particle interactions on a semi-classical level was carried out by Cline, Mostoslavsky and Servant [67], who solved the relativistic Boltzmann equation with QCD and QED interactions in the relaxation-time approximation. They found that significant particle scattering would lead to a photosphere, though not perfect fluid flow.

Daghigh and Kapusta [68] applied relativistic viscous fluid equations to the problem when the Hawking temperature exceeds 100 GeV. They found that a self-consistent description emerges of an outgoing fluid or wind from the black hole which is just marginally kept in local thermal equilibrium, and that viscosity plays a crucial role in the dynamics. A sizable fraction of the total luminosity from the photosphere (which can be many orders of magnitude greater in radius than the Schwarzschild radius) is in the form of photons. They calculated the instantaneous and time integrated photon flux. Using the present upper limit on the rate density of microscopic black holes of about  $1 \text{ pc}^{-3} \text{ yr}^{-1}$  in our neighborhood, they showed that the diffuse spectrum is unlikely to be detectable above other sources. A much more promising route is the search for individual explosions. Assuming no new physics beyond the standard model, a black hole with a temperature of 100 GeV will disappear within 5.4 days. Between 5.4 days and the final 10  $\mu\text{s}$  the average photon energy will increase from 4 to 160 GeV. The signal would be a source which gets brighter over a period of several days and then suddenly disappears. This would be a very unusual event. The maximum reach of a detector which has a

threshold for photons of  $E_{\min}$  and an effective area of  $A_{\det}$  is

$$d_{\max} \approx 150 \sqrt{\frac{A_{\det}}{1 \text{ km}^2}} \left( \frac{10 \text{ GeV}}{E_{\min}} \right)^{3/2} \text{ pc}. \quad (9)$$

The above formula is valid for  $E_{th} > 10 \text{ GeV}$ . If we take the local rate density of explosions to be  $0.4 \text{ pc}^{-3} \text{ yr}^{-1}$  (the current upper limit) then within 1 pc of Earth there would be  $\sim 1.5$  explosions per year. These would be distributed isotropically in the sky. Still, it suggests that the direct observation of exploding black holes may be feasible if their abundance is near the inferred upper limit.

## F. Constraints on Quantum Gravity and Large Extra Dimensions

Theories of quantum gravity, though incomplete, often seem to result in violations of some of the pillars of modern physics including Lorentz invariance, and without some care, even causality. Most theories of the small-scale structure of spacetime lead to dispersion relationships for light traveling in vacuum. The energy dependence of the velocity of light from such relationships is not to be confused with photon mass, which gives the opposite sign. Instead, photons with energies approaching some characteristic TeV to Planck scale are retarded either through the exchange of a Planck scale particle present in quantum gravity, or through distortions in the metric on small distance scales [69]. This violation of Lorentz invariance may be manifested as an energy dependent velocity of light. For many theories of quantum gravity the velocity of light can be parameterized as

$$v \approx c \left( 1 - \zeta \frac{E}{E_{QG}} \right), \quad (10)$$

where  $E_{QG}$  is an energy scale related to quantum gravity and  $\zeta$  is of order 1 and we have ignored terms of higher order in  $E/E_{QG}$ . Since  $E_{QG}$  is expected to be quite large (of order the Planck mass) there seems to be little hope of measuring this effect with earth-bound experiments. To measure small velocity differences one needs short pulses of very high-energy photons traveling cosmological distances.

The above equation leads to a measured time delay for photons of energy  $E_1$  and  $E$  of

$$\Delta T \approx \zeta \frac{LE}{cE_{QG}} \quad (11)$$

if  $E$  is much larger than  $E_1$ . Thus a figure of merit for such measurements is  $LE/\Delta t$ . There are two known sources with reasonable figures of merit: gamma-ray bursts (GRBs) and active galactic nuclei. As discussed above GRBs are short intense bursts of gamma rays that are visible across the visible universe. Active galaxies, while closer, still lie at relatively large distances, and exhibit large short term flux variations. For example, Fig. 15 shows a half-hour flare of TeV photons from an AGN at a distance of 100 Mpc (Mrk 421) observed with the Whipple gamma-ray telescope. These systems make ideal laboratories for studying the constancy of the velocity of light. A difficulty in using GRBs to measure this dispersion is that there are only a few bursts for which the redshift is known and the energy at which these bursts have been observed is typically  $\lesssim 100 \text{ keV}$ . To date the best limit on quantum gravity has been set by the Whipple collaboration [70]. In May 1996 the active galaxy Mrk421 ( $z = 0.031$ ) emitted a flare that lasted for 280 seconds. By examining the arrival time of low ( $\lesssim 1 \text{ TeV}$ ) and high ( $\gtrsim 2 \text{ TeV}$ ) energy data they established a lower limit to  $E_{QG}$  of  $6 \times 10^{16} \text{ GeV}$ . However, this limit assumes that the higher energy photons were not emitted substantially earlier than the lower energy photons. While such an effect is not predicted, there is at present no way of ensuring that an effect due to quantum gravity wasn't partially masked by details of the source; this points to the necessity of understanding the astrophysics of the source to make robust constraints. More recently Ellis et al. [71] have used a sample of GRBs from different redshifts to set a lower limit  $E_{QG} > 10^{15} \text{ GeV}$ . Observations of rapid high energy flares from distant AGNs and GRBs with instruments such as GLAST, Milagro, and VERITAS should improve the current limits by several orders of magnitude and may even reach the Planck scale.

As with all astrophysical measurements it will be crucial to understand the sources of the photons. In this instance, one must be sure that the higher energy photons were not emitted earlier than the lower photons on timescales of seconds. While this seems to be a formidable task, by making measurements of identical (or similar sources) at different redshifts (GRBs), and by measuring the same effect in a different type of source (AGNs), one should be able to make an unambiguous measurement of the effect, even without completely understanding all of the complications of the emission mechanism at the source.

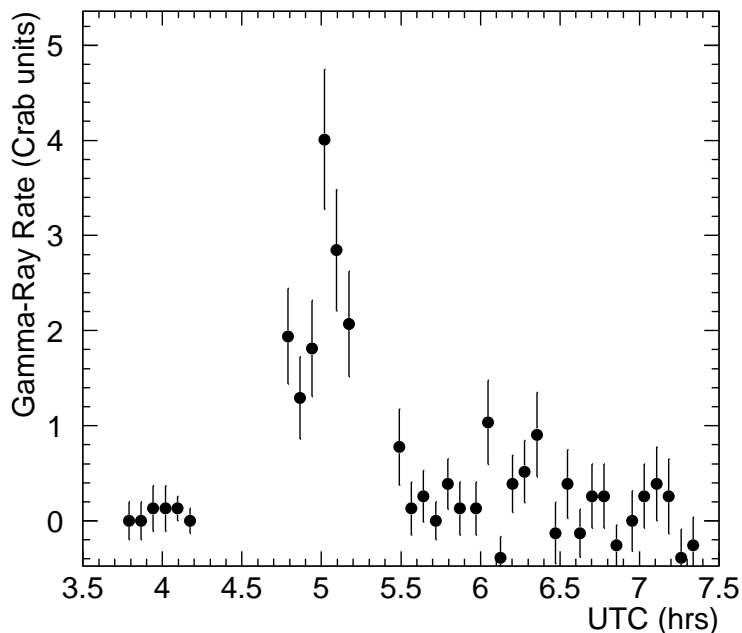


FIG. 15: Mrk 421 flare observed on May 15, 1996 (reprinted with permission of *Nature* 383, 26 September 1996, pp. 320-321; ©1996 Nature Publishing Group[72])

### III. TECHNIQUES OF GAMMA RAY ASTRONOMY

The flux from all known sources of gamma rays falls rapidly with energy. For example the flux of photons from the Crab nebula is  $\sim 0.01 \gamma' sm^{-2} s^{-1}$  above 100 MeV but only  $\sim 10^{-7} \gamma' sm^{-2} s^{-1}$  above 1 TeV. The earth's atmosphere is opaque to high-energy photons (above the ultraviolet), but higher energy photons generate cascades in the atmosphere (extensive air showers), which are detectable from the ground. At lower energies ( $\sim 100$  GeV) the Cherenkov radiation generated by the electromagnetic particles in the shower can be detected by air Cherenkov telescopes (ACTs), and at higher energies sufficient numbers of particles survive to the ground to be directly detected by extensive air shower (EAS) arrays. At lower energies direct measurements with space-based instruments have been used. Over the past decades great progress has been made in extending the energy reach of space-based instruments, with GLAST expected to have sensitivity beyond 100 GeV, and lowering the energy threshold of ground-based instruments. A decade ago the Whipple ACT had an energy threshold of  $\sim 450$  GeV, today experiments utilizing solar power plants, such as STACEE and CELESTE, have achieved energy thresholds below 100 GeV. As for detectors that directly detect the particles on the ground, a decade ago instruments had achieved energy thresholds of  $\sim 100$  TeV. Today, the Milagro EAS array has an energy threshold below 1 TeV.

The other critical feature of gamma-ray telescopes is their ability to reject the cosmic-ray background, which is orders of magnitude larger than the observed gamma-ray signals. The space-based instruments can be surrounded by anticoincidence shield and track the electron positron pairs, providing a straightforward and powerful means of rejecting the cosmic-ray background. For ground-based instruments, the equivalent of an anticoincidence shield does not exist and a detailed understanding of the development of hadronic and electromagnetic showers is used to reject the background. Progress has been slow, but steady improvements have been made. The first generation of ACTs and EAS arrays did not utilize any background rejection and did not convincingly detect any cosmic sources of gamma rays. It was the landmark development of the "imaging" technique, originally proposed by Weekes and Turver [2] that revolutionized the field of ground-based gamma-ray astronomy. Modern ACTs utilizing this technique can remove over 99.7% of the cosmic-ray background yielding unprecedented sensitivity in this energy range. EAS arrays used shielded detectors to detect the penetrating component (muons and hadrons) of hadronic air showers. While this technique has been used for several decades, Milagro is the first instrument to utilize this method in at low primary energies, where one expects to observe sources of gamma rays.

In this section we give a brief history of the various instrumentation used in gamma-ray astronomy, discuss the next generation instruments that are currently under construction, and give a recommendation for the

future development of the field. In the field of particle physics, new discoveries have been dependent upon the construction of new machines, capable of attaining ever-higher energies. The situation is similar in astronomy and in gamma-ray astronomy in particular. We have seen how the development of new techniques has lead to new discoveries and insights into the universe. It is clear that to continue along the path of discovery we must develop new instruments, capable of seeing further into the cosmos (low energy threshold) , and observing the entire sky with much greater sensitivity, to detect and study the transient phenomena that pervade the TeV universe.

### A. Space-Based Experiments: EGRET and GLAST

Above a few MeV, the gamma-nucleus cross section is dominated by pair conversion, which dictates that instruments in this energy range be designed to detect and reconstruct the electron positron pair direction and total energy.

The useful energy range of such a “pair telescope” is determined by the pair-production cross section (at the low end) and counting statistics (at the high-energy end). Although the threshold for pair creation is 1 MeV, the cross section is not significant until 50 MeV, and the threshold for meaningful detection is usually quoted as 20 MeV. The angular resolution is very poor at this energy, however, with 100 MeV being a more practical lower limit for the study of point sources.

The highest energy is limited by flux. With an effective cross sectional area of  $\sim 1 \text{ m}^2$ , the rate of photons from the Crab nebula above 300 GeV is  $10^{-6} \text{ m}^{-2} \text{ s}^{-1}$ . For a year’s direct observation in a detector with  $1 \text{ m}^2$  effective area, the largest practical area for a satellite, this corresponds to about 25 photons per mission, just enough for a “ $5 \sigma$ ” detection.

The three requirements of photon conversion, reconstruction of the pair or subsequent shower, and measurement of the energy, lead to a configuration shared by EGRET and the proposed GLAST: a front section with thin converters interleaved with tracking system; followed by a calorimeter section.

The limiting sensitivity of  $10^{-6} \text{ m}^{-2} \text{ s}^{-1}$  should be compared with the rate for cosmic rays and albedo protons and electrons to intersect the detector, which is around 5 kHz, or some nine orders of magnitude larger. The maximum rate at which data can be transmitted to the ground dictates the efficiency of the hardware trigger. For an average telemetry rate of about 50 Hz, the instrument have a trigger that rejects 99% of incoming cosmic rays with high efficiency for gammas. This requires a third system, namely an outer shield to detect incoming charged particles.

#### 1. EGRET

The Compton Gamma Ray Observatory, including EGRET, was launched in 1991. The EGRET tracking system used 1 mm pitch wire spark chambers with core readout. This technology had several important consequences, including 100 ms deadtime for recharging, and a need for a very strict trigger to limit use of the consumable spark chamber gas and ensure that the trigger rate was consistent with the bandwidth for transmission to ground.

The EGRET trigger had two components: a requirement that there be no count in a monolithic anticoincidence shield surrounding the instrument, and coincidence between two planes of counters between the tracking and calorimeter sections, separated by 30 cm so that the direction could be determined by time of flight.

The EGRET trigger design produced an additional constraint on the maximum gamma-ray energy beyond the simple statistics limit. Since the anticoincidence could be triggered by “back splash” from particles escaping from the calorimeter (a set of NaI crystals), high energy events could produce a *self veto*. This self-veto limited its high energy to about 10 GeV. The need for the time of flight trigger resulted in lengthening the instrument, which in turn limited its field of view.

#### 2. GLAST

GLAST is scheduled for launch in early 2005. The payload is primarily a pair conversion telescope, (Large Area Telescope, or LAT) with a small gamma-ray burst monitor. The design has the same elements as EGRET, but has significantly better performance as a result of modern solid-state technology.

The most important difference is that the tracking section uses silicon strips detectors with 200  $\mu\text{m}$  pitch. This allows dramatic improvements of the deadtime, aspect ratio and therefore angular acceptance, angular resolution at high energy, and high energy acceptance.

Since the tracking system can be read out in a few  $\mu\text{s}$ , and doing so involves no consumables, there is no penalty for a loose first-level trigger. The data can then be analysed and filtered on board before it is transmitted to the ground. Thus it is feasible to trigger on all incoming particles, with rates up to 10 KHz, without using the anticoincidence system in the fast trigger. Like the anticoincidence system of EGRET, GLAST is surrounded by scintillator, but is composed of an array of individual counters rather than a single monolithic dome. Thus the filtering can be selective, in two respects not possible with EGRET: first, if a track candidate determined by the rough on-board track recognition software does not extrapolate to a counter with a signal, it is not vetoed. Second, if the total energy deposited in the calorimeter section is large, the presence of anticoincidence signals will be ignored, avoiding the self-veto possibility.

The resulting increase in the dynamic range of GLAST, improved background rejection with its higher resolution tracker, substantially wider field of view and low dead-time detectors results in more than an order of magnitude improvement in sensitivity compared with EGRET.

### B. Extensive Air Showers

When a high energy gamma ray enters the earth's atmosphere it loses energy by creating an electron positron pair. These particles then lose energy via bremsstrahlung, producing more high energy photons. Until the average energy per particle reaches 80 MeV, particle creation processes dominate the energy loss mechanisms of electromagnetic particles. When the average particle energy reaches 80 MeV, ionization losses dominate and the number of particles in the shower begins to decrease; this point in the development of the air shower is called shower maximum. The particles travel in a rough pancake, that has a  $\sim 100$  m radius and  $\sim 1$  m thickness when it reaches the ground. Figure 16 shows the longitudinal development of extensive air showers of various energies. These curves show the average number of electrons in an extensive air shower as a function of atmospheric depth. At ground level high-energy photons outnumber electrons by a factor of  $\sim 4$ . The development of a single air shower is dominated by fluctuations in the development of the shower. The dominant fluctuation being the depth of the first interaction.

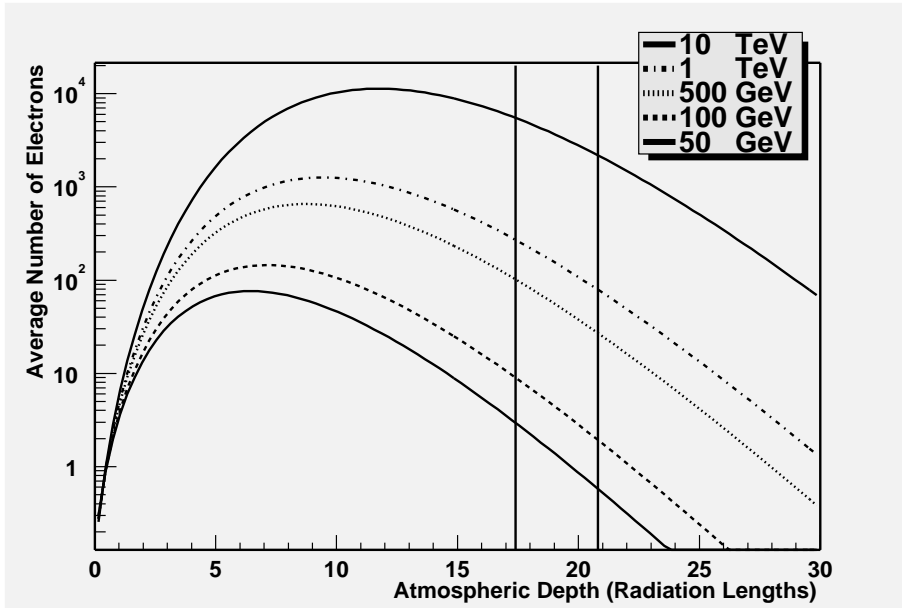


FIG. 16: Shower development curves as given by an approximate semi-analytical expression. The curves show the average number of electrons (and positrons) as a function of atmospheric depth for various energy primary gamma rays. The vertical lines are drawn at 4000 m asl and at 2600 m asl.

### C. Air Cherenkov Telescopes

At present, the most successful ground-based technique employs imaging atmospheric Cherenkov telescopes (IACTs) in which a large optical reflector and a pixelated fast photomultiplier tube (PMT) camera is used to

record the images of electromagnetic cascades. The imaging information can be used to efficiently reject the large background of cosmic-ray showers by making use of the characteristic differences of the hadronic and purely electromagnetic showers (see Fig. 17). The fast time structure of the Cherenkov pulses ( $\sim$  a few nsec) is exploited to detect the faint flashes above the Poisson fluctuations of the night sky background light. The power of this technique comes from the fact that the effective area is much larger than the geometric area of the instrument, and is given instead by the size of the Cherenkov light pool at ground level. Depending on the zenith angle (and distance to shower maximum) this gives an effective area from 10,000 m<sup>2</sup> to 0.1 km<sup>2</sup>. The total amount of Cherenkov light detected provides a reasonably good calorimetric measurement giving an energy resolution of 25% to 40% for a single telescope. While a single telescope provides hadronic rejection with an efficiency of  $\sim$ 99.7%, arrays of telescopes can do substantially better by using stereoscopic imaging to better discriminate hadronic showers. These instruments also provide better angular resolution, more precise energy measurements, and a level of redundancy critical to quantify systematic errors. The prototype for virtually all of the current and proposed IACTs is the Whipple Observatory 10 m telescope located on Mt. Hopkins in southern Arizona [73]. Newer instruments include CAT, a telescope in the Pyrenées operated by a French collaboration [74], CANGAROO, a Japanese-Australian telescope in Woomera, Australia [75], the HEGRA five telescope array operated by an Armenian-German-Spanish collaboration on La Palma in the Canary islands [76].

The STACEE and CELESTE experiments also detect gamma rays by detecting Cherenkov light. Instead of imaging the Cherenkov flashes with an optical telescope, these detectors employ large arrays of heliostats at solar power plants to measure the lateral distribution and to minimize the energy threshold. STACEE currently uses a number of heliostats of 37 m<sup>2</sup> area each focused onto a PMT located in a central tower and read out by a GHz flash analog to digital converter. The direction of the shower front is determined by the relative signal delays in the PMTs. This technique provides a huge mirror area and hence a substantial improvement (proportional to the square root of the mirror area) in the signal to noise ratio for detecting Cherenkov flashes against the night sky background. The energy threshold is limited by this signal to noise ratio as well as by practical limitations in the trigger electronics, but STACEE and CELESTE are already achieving thresholds below of 75 GeV. Upgrades (now well underway) should result in reduced energy thresholds  $\sim$ 30 GeV for both instruments. The shape of the shower front will provide some rejection of hadronic background, but this rejection factor is still to be determined and probably will not reach that of a single imaging ACT. But the low energy threshold and large effective area hold promise for the detection of pulsars, AGNs and other objects.

#### D. Extensive Air Shower Arrays

Extensive air shower arrays directly detect the particles that reach the ground. The direction of the primary gamma ray is determined by measuring the relative arrival time of the air shower over a large area. Figure 17 shows the relative arrival time of the shower front in the Milagro detector. Until recently EAS arrays consisted of sparse arrays of plastic scintillators spread over large areas. Typical physical coverage was between 0.5% (the CYGNUS array) and 1% (the CASA array). With such a small sampling of the air shower, thousands of particles needed to reach the ground to reconstruct the air shower. These arrays were sensitive to primary photons with energies above  $\sim$  100 TeV. There are two techniques to lower the energy threshold of EAS arrays. The technique developed by the Milagro collaboration is to make the entire detector area active. This is accomplished at a reasonable cost by using water as the detecting medium. Since the Cherenkov angle in water is 41° a layer of photomultiplier tubes (PMTs) at a depth comparable to their spacing can detect a particle that enters anywhere in the detector. In addition if the layer of water above the PMTs is several radiation lengths, the more numerous photons in the air shower will convert to electrons and/or positrons above the PMTs and can be detected. The other approach is to place the array at very high altitude. As can be seen in Figure 16, nearly five times as many electrons are present for the same energy shower at 4km asl as at 2.6km asl. The Tibet array has pioneered this approach.

##### 1. Background Rejection in Extensive Air Shower Arrays

A fundamental problem in performing gamma-ray astronomy from the ground is differentiating extensive air showers generated by primary gamma rays from those generated by hadronic cosmic rays. The techniques developed by Weekes and Turver for air Cherenkov telescopes has had great success. The situation in EAS arrays is not as well developed. The primary technique used in EAS arrays has been to detect the penetrating component (mainly muons and hadrons) present in hadronic air showers. The Milagro detector has a second layer of PMTs located beneath 6 meters of water for this purpose. The techniques developed to date yield a

This figure is available as p42\_fig17a.gif

This figure is available as p42\_fig17b.gif

FIG. 17: Events from two varieties of ground-based gamma-ray detectors discussed in the text. *Left*: Measured arrival time of particles in an extensive air shower array in the Milagro detector. The height of the vertical lines represents the time in nanoseconds. The lines are to scale (1 foot = 1 ns). *Right*: Events from the 109 pixel camera on the Whipple telescope (circa 1995). From left to right, top to bottom the first image is that of a candidate gamma-ray (pointing to the putative source the center of the field), an accidental trigger from Poisson fluctuations in the night sky background light, a hadronic shower from a cosmic-ray event, and a ring image from a single muon.

factor of  $\sim 1.8$  improvement in sensitivity [77], denoted as the  $Q$ -factor. This technique depends on the ability to measure the energy deposited in the detector and thus favors thick, calorimetric instruments.

By densely sampling the particles that survive to ground level, non-calorimetric instruments may also reject the hadronic background. Gamma-ray induced air showers tend to have a smooth particle distribution with a well localized core. Hadronic showers exhibit clumps of particles on large and small scales. Applied to a relatively small detector ( $5,000 \text{ m}^2$ ) this technique could give sensitivity improvements comparable to that achieved with Milagro [78],  $Q \sim 1.8$ . Figure III D 1 shows the expected sensitivities of current and planned instruments. For the air shower arrays (Milagro, Tibet, and ARGO) the integration time is 1 year. For the air Cherenkov instruments the integration time is 50 hours on the source (which is a typical amount of time spent on a given source in a year). The sensitivity shown for ARGO assumes no background rejection, and should be viewed as a conservative preliminary estimate [79].

This figure is available as p42\_fig18.gif

FIG. 18: Expected sensitivity of current and planned instruments.

#### IV. FUTURE EXPERIMENTAL DIRECTIONS

What is the logical follow-up to the current experiments that will facilitate the best scientific return? A reduction in energy threshold of conventional ACTs would increase overlap with GLAST, and would extend the gamma-ray horizon allowing the detection of more distant extragalactic sources and GRBs. However, conventional imaging ACTs are narrow field instruments for which observations must be guided by some other source of information (GLAST source locations, X-ray surveys). For flaring sources, a trigger from a wide-field instrument is required and the time to slew a large telescope may well exceed the most interesting timescale. To achieve sensitivity to the shortest AGN flares, to provide continuous coverage of the rapidly varying emission, to provide spectral cutoffs for a large ensemble of AGN, and to catch short and long-duration GRBs during their development requires a global network of very wide field instruments instrument with very good sensitivity to  $E > 100 \text{ GeV}$  events, and optimized for temporal coverage rather than point source sensitivity.

The current generation of space-based gamma-ray detectors (AGILE and GLAST) will provide all-sky coverage and good sensitivity to both point sources and diffuse emission at energies above 100 MeV. Above 50 GeV,

HESS, VERITAS and other ground-based atmospheric Cherenkov detectors will provide the high point source sensitivity and huge effective areas (more than  $\sim 10^4$  times that of satellite experiments) required to study the shortest variability time-scales and to provide time-resolved spectra from 50 GeV up to 50 TeV. Arrays of imaging atmospheric Cherenkov detectors now under construction (e.g., VERITAS in the northern hemisphere and HESS in the southern hemisphere) complement GLAST. Jointly these experiments are assured to make major strides in astrophysics.

## A. Atmospheric Cherenkov Instruments

### 1. High Sensitivity: VERITAS and HESS

VERITAS is a proposed array of seven 10m aperture optical reflectors that combines the best elements of the large aperture Whipple telescope, with the power of stereoscopic imaging pioneered by the HEGRA collaboration. VERITAS will have good sensitivity in the energy range 50 GeV to 50 TeV energy range. To quote a typical figure of merit, for observations of the Crab nebula the peak counting rate will be obtained at about 75 GeV. Each VERITAS telescopes will use the imaging concept developed by the Whipple Observatory Gamma-Ray Collaboration and used to detect the first galactic and extragalactic sources of TeV  $\gamma$ -rays but will achieve an order of magnitude better sensitivity and a significant reduction in energy threshold to 75 GeV. The new telescopes will improve upon the design of the existing 10 m  $\gamma$ -ray telescope. Each telescope will have a tessellated 10 m mirror and long focal length (12 m) with the optical design optimized for good angular resolution, a large field of view, minimum wavefront distortion and identical, spherical mirror facets. Each telescope camera will have 499 pixels covering a  $3.5^\circ$  field of view with  $0.15^\circ$  resolution. The detectors and camera electronics will use high speed 500 MHz flash ADCs, and a low time jitter intelligent trigger. The array will have an effective collection area in excess of  $40,000 \text{ m}^2$ . VERITAS will be located in southern Arizona where it will take advantage of the existing infrastructure of the Whipple Observatory/ With stereoscopic imaging, the array will achieve an unprecedented angular resolution, energy resolution and background rejection over three decades of energy. The primary scientific objectives of VERITAS will be the study of active galactic nuclei, supernova remnants, pulsars,  $\gamma$ -ray bursts, and the search for new sources. The minimum detectable flux sensitivity will be 0.5% of the Crab Nebula at 200 GeV, a factor of 20 improvement over the Whipple telescope, the most sensitive telescope currently operating in this energy range. The angular resolution ( $<0.05^\circ$ ) will be sufficient to identify a number of the unidentified sources detected by EGRET on the Compton Gamma Ray Observatory. A simple extrapolation suggests that more than 30 active galactic nuclei will be detected. VERITAS provides a unique combination of large collection area, low background, and good energy resolution.

### 2. Low Energy Threshold: 5@5

The “5@5” Cherenkov telescope array is a design concept for a ground-based gamma-ray telescope system that will bring the enormous  $\sim 10^4 \text{ m}^2$  meter collection area that Cherenkov telescopes enjoy at TeV energies down to the GeV energy range. Currently, the GeV energy range is accessible only to space-based instruments like EGRET and the future GLAST. While such instruments have wide fields of view and thus are well-suited for surveys, they also have inherently small collection areas ( $\sim 1 \text{ m}^2$ ) and thus are not well-suited for monitoring sources that exhibit strong GeV variability on second to hour timescales, e.g., gamma-ray bursts and blazars. Being able to follow this rapid variability is crucial for constraining the emission mechanisms and physics conditions in these sources.

Referring to Fig.IIID 1, the sensitivity curves for 5@5 (ground-based) and GLAST (space-based) would cross at 10 GeV. Note, though, that the source integration times are very different for the two instruments. The integration times used (50 hours vs. 1 year or *sim*9000 hours) are chosen as the maximum total times one can easily acquire on a source during one observing season. (Ground-based instruments have a much lower duty cycle because they only operate in dark conditions.) For the detection of a new, steady source, the two instruments are comparable in capabilities. However, the ground-based telescope has acquired its photons in a time interval that is  $\sim 200$  times shorter – a crucial advantage when one is dealing with rapidly varying sources. While a 5@5-class instrument and GLAST may appear to be competitors and perhaps redundant, they are in fact highly complementary. Cherenkov arrays are narrow field instruments and the sky density of transient gamma-ray sources is very low, i.e., a 5@5 instrument requires a wide-field instrument like GLAST to tell it where to point. A low threshold experiment such as 5@5 and GLAST provide two complementary approaches to achieving some of the most important scientific objectives: GLAST would be ideal for surveys and 5@5 for deep studies of spectral and temporal characteristics of gamma-ray sources. In particular, 5@5 would be an



excellent instrument for study of variable/transient gamma-ray phenomena (blazars, microquasars, and long duration GRBs) if a wide-field trigger is available. To put the capabilities of such an instrument in perspective, consider a transient source with the flux of the Vela pulsar; such a GeV transient source could be detected by 5@5 for just 1 second exposure time! The rapid development and successful operation of a low-threshold Cherenkov telescope during the lifetime of GLAST would therefore represent a major observational coup.

Another route to such improvements in energy threshold would be to upgrade VERITAS, HESS or MAGIC with higher quantum efficiency detectors. Current employed bialkali PMTs have quantum efficiencies of  $\sim 20\%$ , while semitransparent InGaN or reflection-mode GaAsP solid state cathodes promise to double or triple the efficiency.

To lower the energy threshold, the collection efficiency of Cherenkov photons must be dramatically improved. Barring some fundamental breakthrough in detector quantum efficiency there are only two ways to increase the collection: (i) build a much larger, more expensive telescope mirror, or (ii) use smaller, cheaper mirrors but go to higher altitudes where fewer Cherenkov photons suffer atmospheric absorption. The first approach represents the strategy employed by the MAGIC collaboration (a single large 17 meter mirror at an altitude of 2000 meters), while the second is the one behind the proposed 5@5 concept (5 12 meter mirrors at an altitude of 5000 meters operating in a stereoscopic configuration). The advantages of operating at high altitude are several. First, the amount of Cherenkov light per gamma-ray primary is higher. This allows one to detect a Cherenkov pulse with a smaller mirror, and thus it becomes feasible to consider the construction of several of these mirrors. When placed in a suitable array configuration (in the 5@5 design, four mirrors are placed at the corners of a square and one telescope is placed at the center), these telescopes can be jointly triggered and operated stereoscopically. Even in the  $\sim 10 - 100$  GeV regime where the gamma-ray shower shape becomes less well-defined, this allows for a much cleaner rejection of cosmic ray and muon backgrounds than is possible with a single telescope. An additional advantage of going to higher altitudes is that the cosmic-ray induced background is intrinsically lower to begin with because cosmic-ray showers tend to peak at lower altitudes. At energies below  $\sim 100$  GeV and at high altitudes, one can therefore operate in a mode where effectively background comes only from cosmic ray electrons. This background can be readily measured and removed in the same way one subtracts the night sky background in optical CCD images. Note also that at very low energies this electron background can be minimized by the appropriate choice of site location. The proposed 5@5 site in Chile has a geomagnetic latitude such that the low-energy electron rigidity cutoff there is 15 GeV, i.e., the background at lower energies may be strongly suppressed leading to a corresponding gain in sensitivity. The proposed location of the 5@5 array in the Atacama desert plateau also overcomes the one major disadvantage that has hampered previous attempts at high altitude arrays, namely the combination of bad weather and the sheer physical difficulty of operating in a high altitude environment. The Atacama desert is one of the best astronomical sites in the world (with stable atmospheric conditions and low cloud cover), and it already has excellent support infrastructure because of the large, international millimeter array (ALMA) that is currently being built there.

## B. Large Field-of-View Instruments

The development of a ground-based gamma ray instrument with a large field-of-view and good sensitivity (comparable to that projected for VERITAS) should be a high priority. This is required for the observation of flaring AGN and perhaps more importantly to observe the high-energy emission from gamma ray bursts. At present there are two possible approaches. The development of wide field optics is a requirement of the OWL instrument (a space-based instrument to detect the fluorescence in the atmosphere from ultra-high-energy cosmic rays). Similar technology could be used in ground-based air Cherenkov telescopes. Alternatively, one can build a large area, dense sampling, extensive air shower array at high altitude. Both techniques require further development.

### 1. Large Field-of-View Air Cherenkov Instruments

To achieve simultaneous coverage of a large portion of the sky, instruments with fields of view of 30 to 60 degrees will be required. Reflective optics are limited to about 15 degree fields of view, above which the secondary (or tertiary) optics grow to the point that the entire primary is obscured! Technical innovations such as refractive optics (UV transparent Fresnel lenses), large area megapixel detectors, high speed ASICs, and new data handling capabilities will be required to make such an instrument. Limitations in the size of Fresnel optics may also necessitate higher quantum efficiency detectors to achieve a target threshold approaching 100 GeV.

An impetus for this work comes from the proposal to build a downward looking atmospheric fluorescence

detector (OWL or EUSO) to detect ultra-high energy cosmic rays and neutrinos. This technologically bold proposal would require the deployment of 3 to 10m optics in space, with megapixel cameras covering the same area. Future ground-based gamma-ray experiments and d space-based atmospheric fluorescence detectors have some remarkable similarities in their technological requirements. Both require wide-field (10-60 degree) optics, large apertures (10m), high quantum efficiency UV/blue photon-counting detectors, cameras with large plate scales and large numbers of pixels (up to 1 million) and inexpensive ASICs for time-digitization of signals. Collaborations between the gamma-ray and ultra-high energy cosmic ray communities are a logical step to develop the enabling technologies.

## 2. Extensive Air Shower Arrays

The development of high-sensitivity extensive air shower arrays is a nascent field. To date the Milagro instrument is the only instrument operating at relatively low energy threshold that has the ability to reject the cosmic-ray background. ARGO is an instrument currently under construction in Tibet, that will also have the ability to reject the cosmic-ray background. Neither instrument approaches the rejection levels now attained in air Cherenkov telescopes. This represents the major challenge for future air shower arrays. The goals of the next generation extensive air shower arrays are to:

1. reach sensitivities (with one year of integration) comparable to those achieved by VERITAS (with 50 hours of on-source integration),
2. have sufficient effective area at or below 100 GeV to see more distant gamma ray bursts (if their spectra continue to these energies).

These goals require that current instruments must undergo a factor of  $\sim 50 - 100$  improvement in sensitivity. The sensitivity to a point source can be calculated with the following formula.

$$S = Q\sigma_{\theta} \frac{\int_{E_{th}}^{\text{inf}} A_{\gamma}(E)E^{-s}dE}{\int_{E_{th}}^{\text{inf}} A_p E^{-2.7}dE} \quad (12)$$

where  $s$  is the differential spectral index of the source,  $A_{\gamma,p}(E)$  is the effective area for gamma rays/protons,  $\sigma_{theta}$  is the angular resolution of the instrument, and  $Q$  is the gain in sensitivity due to background rejection ( $\epsilon_{\gamma}/\sqrt{\epsilon_p}$ ), where  $\epsilon_{\gamma,p}$  is the efficiency for keeping gamma rays/protons). For a Crab like source ( $s = 2.4$ ) and with the assumption that the effective area is a step function one can derive the following figure of merit for EAS arrays:

$$M \approx Q\sigma_{\theta} \frac{R_{\gamma}\sqrt{A_{det}}}{\sqrt{E_{th}}} \quad (13)$$

where  $R_{\gamma}$  is the square root of the ratio of effective areas for gamma rays and protons. The fact that  $R_{\gamma}$  is not unity is a reflection of the differences in the development of gamma ray and proton induced air showers. In general  $R_{\gamma}$  is a function of energy and altitude (or zenith angle of observation). For Milagro, located at 2600 m asl,  $R_{\gamma} \sim 1$ . At 4000m asl  $R_{\gamma}$  is between 1.5 and 2. The dependence on  $E_{th}$  given above is dependent upon the source spectrum.

Examination of Figure 16 shows that for a 100 GeV gamma ray induced air shower there are  $\sim 5$  times as many electrons and positrons at 4000m asl than at 2600m asl. It is clear that any future detector must be located at extreme altitudes. The next requirement is driven by the fact that there are many more photons than electrons present in the air shower. This demands that the detector be “thick”, several radiation lengths, to observe these photons. Using equation 13 one can determine that a Milagro type detector located at 4000m asl and with  $10\times$  the physical area will be roughly 10-15 times more sensitive than the current Milagro instrument. However, the operational experience of Milagro has highlighted several areas where large improvements can be made. These issues are currently being addressed but we believe that they will lead to a factor of 3 improvement in sensitivity. The biggest issue is simply the size of the detector. With an area 5000 m<sup>2</sup> and high sensitivity to individual particles, most of the showers (80%) that trigger the detector have their cores outside of the pond. This leads to a degradation in the angular resolution of the instrument. An array of 170 water tanks is currently being built around the main pond to locate the shower core for these events. Monte Carlo simulations indicate that this should improve the sensitivity of Milagro by a factor of 2, this comes both from improved angular resolution and improved background rejection. In addition, the main impediment to lowering the trigger threshold of Milagro is the rate of single muons. Smart triggers should enable one to lower the energy threshold to further improve the

sensitivity by 30%. Thus, there is good reason to expect that such an instrument located at 4000m asl will have a sensitivity  $\sim 30$  times greater than the current Milagro instrument. To make further improvements one needs to improve the background rejection and/or the angular resolution of the instrument. Given the relative infancy of background rejection in air shower arrays, and the great progress made by air Cherenkov instruments in the past decade, this does not seem to be an unreasonable improvement. However, work is needed to demonstrate that such an improvement can be realized.

## V. CONCLUSIONS

The field of gamma-ray astronomy has changed radically in the past decade. In 1990 there were a handful of gamma-ray sources observed from space and only one source observed from the ground. Today there are over 150 known sources of gamma rays observed from space and about 10 sources of TeV gamma rays observed from the ground. The coming decade promises even greater advances. There are new ground-based and space-based instruments currently under development that will increase the number of known sources by over an order of magnitude. Large field-of-view instruments with relatively low-energy thresholds ( $\sim 500$  GeV) capable of detecting very-high-energy emission from gamma-ray bursts are now beginning to acquire data. It is clear that this is still a relatively young field where new ideas are being pursued and large advances are on the horizon.

At the workshop we heard from many participants about current measurements and the increasing overlap with particle physics. The time where distant cosmic sources can be used to probe the fundamental interactions of matter at energy scales unattainable on Earth is approaching. Much discussion centered around possible future directions. Two goals were put forth for ground-based instruments: a very low energy threshold instrument ( $\sim 10$  GeV) and a very sensitive wide-field instrument with an energy threshold  $\sim 100$  GeV. We look forward to the coming decade.

## VI. REFERENCES

- 
- [1] R. C. Hartman and et al., ApJS **123**, 79 (1999).
  - [2] T. C. Weekes and K. E. Turver, in *in Proc. 12th ESLAB Symp.* (Frascati, ESA Sp-124, 1977), p. 279.
  - [3] C. von Montigny and et al., ApJ **440**, 525 (1995).
  - [4] M. Sikora, M. Begelman, and M. Rees, ApJ **421**, 153 (1994).
  - [5] K. Mannheim, A&A **269**, 67 (1993).
  - [6] A. Kerrick and et al., ApJ **452**, 588 (1995b).
  - [7] J. Quinn and et al., in *in Proc. 24th ICRC* (Rome, 1995), vol. 2, p. 369.
  - [8] D. Petry and et al., in *in Proc. 25th ICRC* (Durban, South Africa, 1997), vol. 3, p. 241.
  - [9] M. Punch and et al., Nature **358**, 477 (1992).
  - [10] J. Quinn and et al., ApJ **456**, L83 (1996).
  - [11] M. Catanese, ApJ **501**, 616 (1998).
  - [12] P. M. Chadwick and et al., Astropart. Phys. **11**, 145 (1999).
  - [13] Nishiyama and et al., in *in Proc. 26th ICRC* (Salt Lake City, Utah, 1999), (unpublished communication).
  - [14] D. Horan and et al., in *in Proc. 27th ICRC* (Hamburg, Germany, 2001), p. (in press).
  - [15] P. Padovani and P. Giommi, ApJ **444**, 567 (1995).
  - [16] C. D. Dermer, R. Schlickeiser, and A. Mastichiadis, A&A **256**, L27 (1992).
  - [17] R. Gould and G. Schreder, Phys. Rev. **155**, 1408 (1967).
  - [18] F. Stecker and O. D. Jager, ApJ **415**, L71 (1993).
  - [19] G. Fossati, L. Maraschi, A. Celotti, A. Comastri, and G. Ghisellini, MNRAS **299**, 433 (1998).
  - [20] J. Buckley, in *in Proc. Gamma-2001 Conference* (AIP, Baltimore, MD, 2001), p. (in press).
  - [21] J. Buckley and et al., ApJ **472**, L9 (1996).
  - [22] M. Jordan and et al., in *in Proc. 27th ICRC* (Hamburg, Germany, 2001), p. (in press).
  - [23] G. Fossati and et al. (2001), (in preparation).
  - [24] H. Krawczynski, P. S. Coppi, T. Maccarone, and F. A. Aharonian, A&A **353**, 97 (2000).
  - [25] J. Bahcall and E. Waxman, Phys Rev D **61**, 3002 (2001).
  - [26] F. Aharonian, New Astronomy **5**, 377 (2000).
  - [27] M. Catanese and et al., ApJ **487**, L143 (1997a).
  - [28] J. Buckley and et al., in *in Proc. of the 4th Compton Symp.*, edited by C. Dermer, M. Strickman, and J. Kurfess (AIP, 1997), vol. 410, p. 1381.
  - [29] R. W. Klebesadel, I. B. Strong, and R. A. Olson, Astrophys. J **182**, L85 (1973).

- [30] E. Costa and et al., *Nature* **387**, 783 (1997).
- [31] D. A. Frail and et al. (2001), astro-ph/0102282.
- [32] J. P. Norris, G. Marani, and J. T. Bonnell, *Astrophys. J.* **534**, 248 (2000).
- [33] K. Hurley and et al., *Nature* **372**, 652 (1994).
- [34] G. Jungman, M. Kamionkowski, and K. Greist, *Phys. Reports* **267**, 195 (1995).
- [35] J. Ellis and et al., *Nucl. Phys.* **B238**, 453 (1984).
- [36] L. Bergstroem, J. Edsjo, and P. Ullio, *ApJ* **526**, 215 (1999).
- [37] S. Barwick and et al., *ApJ* **482**, L191 (1997).
- [38] S. Coutu and et al., in *in Proc. 27th ICRC* (Hamburg, Germany, 2001), p. (in press).
- [39] E. Baltz and et al. (2001), astro-ph/0109318.
- [40] L. Bergstrom, P. Ullio, and J. Buckley, *Astropart. Phys.* **9**, 137 (1998).
- [41] P. Côté, C. Carignan, and K. C. Freeman, *AJ* **120**, 3027 (2000).
- [42] W. J. G. de Blok, S. S. McGaugh, A. Bosma, and V. C. Rubin, *Ap. J.* **552**, L23 (2001).
- [43] S. Blais-Ouellette, P. Amram, and C. Carignan, *AJ* **121**, 1952 (2000).
- [44] F. C. van den Bosch and R. A. Swaters, *MNRAS* **325**, 1017 (2001).
- [45] A. S. Font and J. F. Navarro (2001), astro-ph/0106268.
- [46] P. Ullio, H. S. Zhao, and M. Kamionkowski, *Phys. Rev. D.* **64**, 043504 (2001).
- [47] P. Gondolo, *Phys. Lett.* **B494**, 181 (2000).
- [48] P. Gondolo and J. Silk, *Phys. Rev. Lett.* **83**, 1719 (1999).
- [49] J. N. Bahcall and R. M. Soneira, *Ap. J. Suppl.* **44**, 73 (1980).
- [50] M. Persic, P. Salucci, and F. Stel, *MNRAS* **281**, 27 (1996).
- [51] J. F. Navarro, C. Frenk, and S. White, *Ap. J.* **462**, 563 (1996).
- [52] B. Moore et al., *Ap. J.* **499**, L5 (1998).
- [53] M. Kamionkowski and A. Liddle, *Phys. Rev. Lett.* **84**, 4525 (2000).
- [54] J. Binney, O. Gerhard, and J. Silk, *MNRAS* **321**, 471 (2001).
- [55] M. D. Weinberg and N. Katz (2001), astro-ph/0110632.
- [56] M. Milosavljevic, D. Merritt, A. Rest, and F. C. van den Bosch (2001), astro-ph/0110185.
- [57] T. Alexander, *Ap. J.* **527**, 835 (1999).
- [58] K. Kosack and et al., in *in Proc. 27th ICRC*, edited by M. Simon, E. Lorenz, and M. Pohl (Hamburg, Germany, 2001), p. 2989.
- [59] H. Mayer-Hasselwander and et al., *A& A* **335**, 161 (1998).
- [60] S. D. Biller and et al., *Phys. Rev. Lett.* **80**, 2992 (1998).
- [61] V. V. Vassiliev, *Astroparticle Physics* **12**, 217 (2000).
- [62] J. R. Primack, J. S. Bullock, R. S. Somerville, and D. MacMinn, *Astroparticle Physics* **11**, 93 (1999).
- [63] S. W. Hawking, *Nature* **248**, 30 (1975).
- [64] J. MacGibbon and B. R. Webber, *Phys Rev. D* **41**, 3052 (1990).
- [65] A. F. Heckler, *Phys. Rev. D* **55**, 480 (1997).
- [66] A. F. Heckler, *Phys. Rev. Lett.* **78**, 3430 (1997).
- [67] J. M. Cline, M. Mostoslavsky, and G. Servant, *Phys Rev D* **59 no. 6**, 630091/1 (1999).
- [68] R. G. Daghigh and J. I. Kapusta (2001), gr-qc/0109090.
- [69] G. Amelino-Camelia and et al., *Nature* **393**, 763 (1998).
- [70] S. D. Biller and et al., *Phys. Rev. Lett.* **83 no. 11**, 2108 (1999).
- [71] J. Ellis and et al., *Astrophys. J.* **535**, 139 (2000).
- [72] J. A. Gaidos and et al., *Nature* **383**, 319 (1996).
- [73] M. F. Cawley and et al., *Exp. Astron.* **1**, 173 (1990).
- [74] A. Barrau and et al., *Nucl. Instrum. Methods A* **416**, 278 (1998).
- [75] T. Hara and et al., *Nucl. Instrum. Methods A* **332**, 300 (1993).
- [76] A. Daum and et al., *Astropart. Phys.* **8**, 1 (1997).
- [77] C. Sinnis, in *in Proc. of the 27th ICRC* (Hamburg, Germany, 2001), p. (in press).
- [78] S. Bussino and S. M. Mari, *Astropart. Phys.* **15**, 65 (2001).
- [79] B. D. Piazzoli, Private Communication (2001).

This figure "p42\_fig1a.gif" is available in "gif" format from:

<http://arxiv.org/ps/astro-ph/0201160v1>

This figure "p42\_fig2.gif" is available in "gif" format from:

<http://arxiv.org/ps/astro-ph/0201160v1>

This figure "p42\_fig5.gif" is available in "gif" format from:

<http://arxiv.org/ps/astro-ph/0201160v1>

This figure "p42\_fig6.gif" is available in "gif" format from:

<http://arxiv.org/ps/astro-ph/0201160v1>



This figure "p42\_fig9.gif" is available in "gif" format from:

<http://arxiv.org/ps/astro-ph/0201160v1>

This figure "p42\_fig11.gif" is available in "gif" format from:

<http://arxiv.org/ps/astro-ph/0201160v1>

This figure "p42\_fig13.gif" is available in "gif" format from:

<http://arxiv.org/ps/astro-ph/0201160v1>

This figure "p42\_fig17a.gif" is available in "gif" format from:

<http://arxiv.org/ps/astro-ph/0201160v1>

This figure "p42\_fig17b.gif" is available in "gif" format from:

<http://arxiv.org/ps/astro-ph/0201160v1>

This figure "p42\_fig18.gif" is available in "gif" format from:

<http://arxiv.org/ps/astro-ph/0201160v1>